Assessment of CSG-induced subsidence in the Surat CMA

(OGIA/21/CD19/V1)

Version 1.0

November 2021

Office of Groundwater Impact Assessment

Version	Release date	Authorised by
1.0	xxx	

Overall guidance and direction:

Prepared by:

Contributors:

Review:

Acknowledgement:

This publication has been compiled by the Office of Groundwater Impact Assessment, Department of Regional Development, Manufacturing and Water.

Interpreter statement:

The Queensland Government is committed to providing accessible services to Queenslanders from all culturally and linguistically diverse backgrounds. If you have difficulty in understanding this document, you can contact us within Australia on 13QGOV (13 74 68) and we will arrange an interpreter to effectively communicate the report to you.

Table of contents

Table of figures

Table of tables

This page is intentionally blank

1 Introduction

1.1 About this document

OGIA undertook a comprehensive assessment of coal seam gas (CSG) induced subsidence to support an assessment of impacts on environmental values (EVs) for the UWIR 2021 (OGIA 2021a). An overview of the assessment is presented in Chapter 7 of the UWIR. This companion document supplements the UWIR 2021 with additional technical details on some elements of the assessment, and therefore, should be read in conjunction. However, for completeness and continuity some parts of the UWIR 2021 are repeated in this report.

1.2 Context and scope

In relation to CSG-induced subsidence various components of assessment, management and potential mitigation can be grouped into three categories and conceptualised as 'triple M' to represent monitoring, modelling and mitigation components (Figure 1-1).

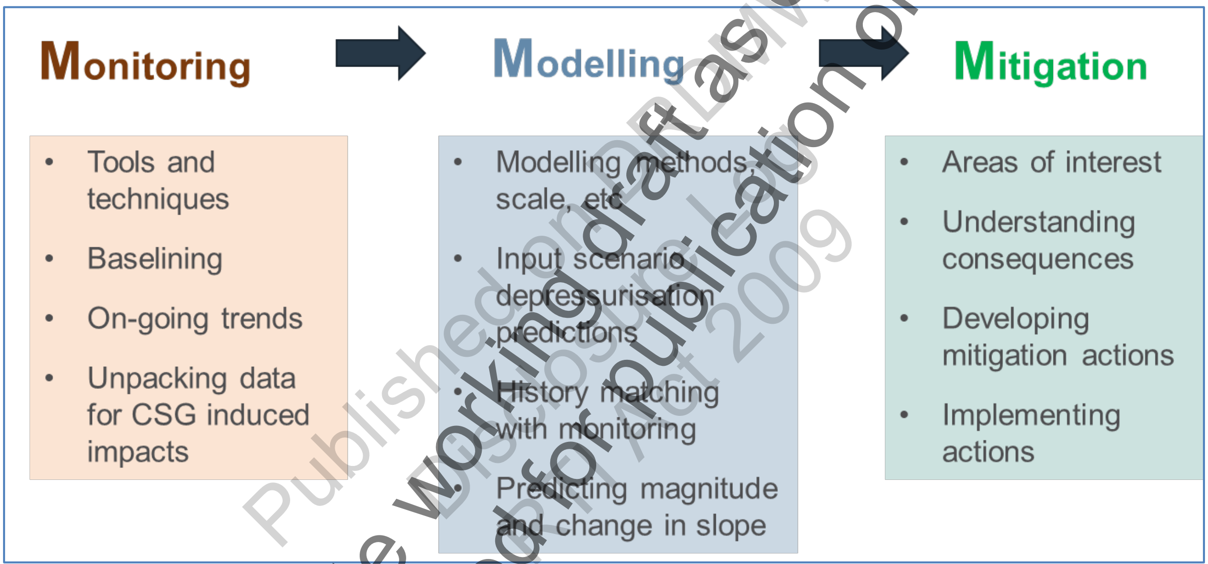

Figure 1-1 'Triple M' – CSG-induced subsidence management categories

In the context of the UWIR, the scope of the subsidence assessment related matters is limited to monitoring and modelling, and specifically excludes follow-up risk assessment, consequences or the development of mitigation actions where necessary.

1.3 Terminology

Ground movement – also referred to as 'ground motion', the movement in ground surface elevation measured at surface, irrespective of the cause.

Subsidence – used in this report to refer to the component of ground movement that is induced by CSG depressurisation.

Ground slope – change in slope of the land at surface resulting from CSG-induced subsidence.

2 Conceptualisation of subsidence

2.1 General

In response to CSG depressurisation (CD CSG xxx), coal seams in the target formation will compact due to the reduction of pressure from the removal of fluids (gas and water). This causes partial collapse of coal cleats that are otherwise held open by the in-situ pore pressure. Some compaction of the rock matrix may also occur due to increased effective stresses.

As a result of the combination of these two factors, the overlying formations may subside, resulting in some subsidence at the ground surface. A schematic of the mechanism for subsidence is shown in Figure 2-1. In addition, when gas is extracted from the coal seam formation, the effect of gas desorption-induced shrinkage may result in additional compaction of the coal seams and subsequent subsidence of land surface.

The primary CSG target formation in the Surat cumulative management area (CMA) is the Walloon Coal Measures. In terms of their relative magnitudes, hundreds of metres of depressurisation in the Walloon Coal Measures will typically result in tens to hundreds of millimetres of subsidence at the ground surface.

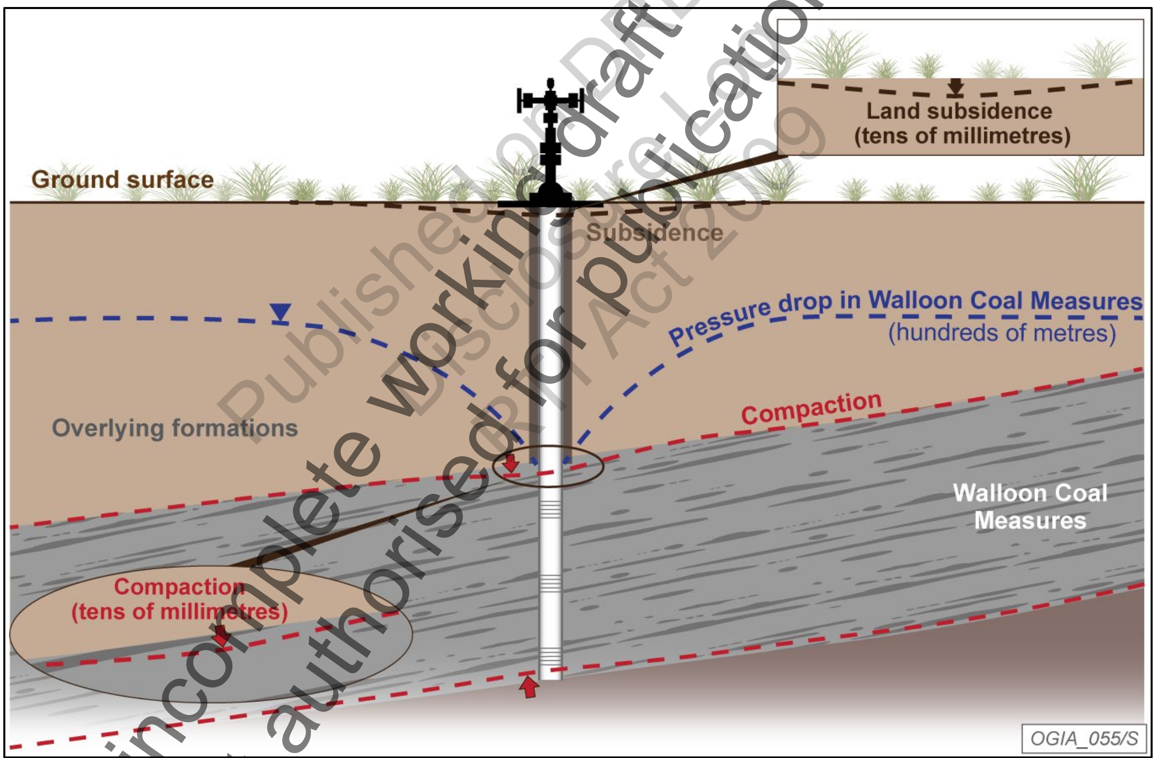

Figure 2-1: Schematic showing the mechanism for CSG-induced subsidence

In the context of the Surat Basin, some of the primary factors that determine the magnitude of subsidence include the (after Commonwealth of Australia 2015):

- magnitude and area of depressurisation
- geomechanical properties of the coal and overlying sediments
- thickness and distribution of coal which is being depressurised

Some of these factors are further detailed in following sections.

2.2 Magnitude and area of depressurisation

The primary factor affecting variations in subsidence - spatially and temporally - is the area and magnitude of pressure decline. This is strongly controlled by the density and distribution of CSG wells, as well as the period of time since each well has been active (OGIA 2021b).

Depressurisation around a single CSG well is greatest closer to the well and decreases laterally away from the well, as shown in Figure 2-1. This is commonly referred to as the ‘cone of depression’. The difference between the initial (pre-pumping) pressure distribution and the pressure distribution at any point after the start of production is referred to as ‘drawdown’. The zone of influence (i.e., how far the drawdown propagates laterally) typically depends on the amount of groundwater extracted, permeability and the storage properties of the formation.

CSG operations tend to target a level of depressurisation in the well that facilitates gas desorption. This is typically 35 to 80 m above the top of the first major coal seam. Regardless of the volume of groundwater extraction, this is the level to which pressure is maintained during production. This is an important concept in the context of subsidence because once the targeted level of depressurisation is achieved at a given location and subsequent compaction occurs, no further significant compaction is expected to occur, even if nearby wells continue to operate.

Multiple CSG wells are operated in a gas field to create widespread and relatively uniform pressure decline (i.e., depressurisation) within the fields to optimise gas production. However, there is a pressure gradient away from the gas fields, extending to about 10 to 15 km from the edge of the CSG fields. This is because of the interference and interaction between the cones of depressions from multiple individual CSG wells.

In the Surat Basin this is achieved by completing vertical wells about 750 m apart, or directional wells with intakes that are about the same distance or less apart underground. This is depicted schematically in Figure 2-2.

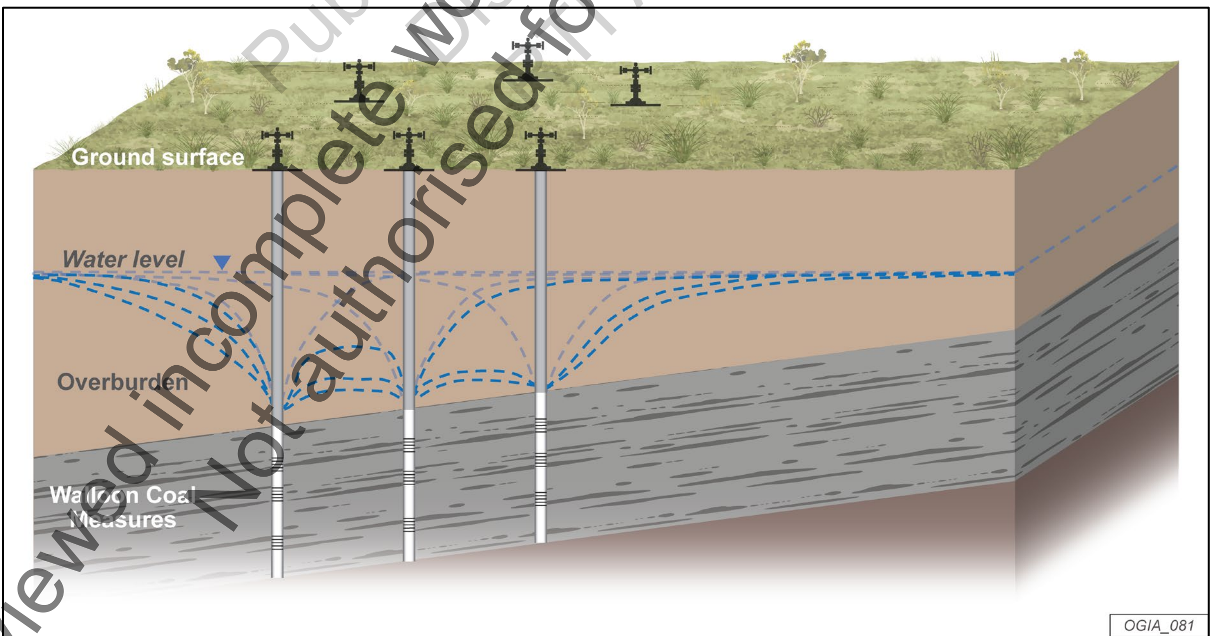

Figure 2-2 Depressurisation pattern resulting from individual CSG wells cone of depressions

Due to the overlap between individual cones of depression from CSG wells, the pattern of groundwater depressurisation within gas fields will be relatively uniform over time. Consequently, this will result in relatively uniform subsidence within the active gas fields, gradually tapering away with distance from the gas fields.

2.3 Geomechanical properties

The magnitude of subsidence is partially controlled by the characteristics of the lithological material within the target coal formation, as well as the overlying strata.

Depressurisation of targeted coal formations during CSG well development and extraction increases the effective stress applied to the targeted and surrounding lithologies by overlying strata. The geomechanical properties of the coal and interburden rocks control how these rocks behave in response to the increased effective stress. As coal is the primary target for CSG extraction and is usually the softer, more compressible rock type present in the formation, compaction is generally most significant within the coal seams of the target formation (Erling Fjær, Rune Holt, Per Horsrud 2008). As discussed in Section 2.1.1, coal compaction occurs within the cleats and matrix of the coal seams.

The degree of subsidence realised at the surface will also depend on the bridging strength of the overburden material which will determine its ability to accommodate the stresses resulting from underlying coal compaction. However, due to the regional extent and magnitude of depressurisation and drawdown, the influence of bridging on subsidence is minimal in the Surat Basin.

2.4 Thickness and distribution of coal seams

As CSG-induced subsidence is largely caused by coal compaction, it is strongly influenced by the thickness and spatial distribution of coal in the target formations.

In and around the Condamine Alluvium the thickness of coal depends on the available thickness of the Walloon Coal Measures, which was eroded and dissected by surface water flows during the deposition of the Condamine Alluvium. Therefore, the Condamine Alluvium unconformably overlies the westward dipping Walloon Coal Measures. As a result, the overall thickness of the Walloon Coal Measures reduces in the east, where the upper most sub-unit (Juandah Coal Measures) becomes absent (Figure X).

We probably already have a schematic like this???

Figure 2-3 Schematic of the contact between the Walloon Coal Measures and the Condamine Alluvium

This inherently reduces the total coal thickness towards the east (see Figure 2-4). As detailed in s4.4.2 of the UWIR 2021 (OGIA 2021a), the Walloon Coal Measures is comprised of numerous thin non-continuous lenses of coal separated by interburden comprised of sandstone, siltstone and mudstone. However, the total proportion of coal generally remains around 9% of the total thickness of the formation

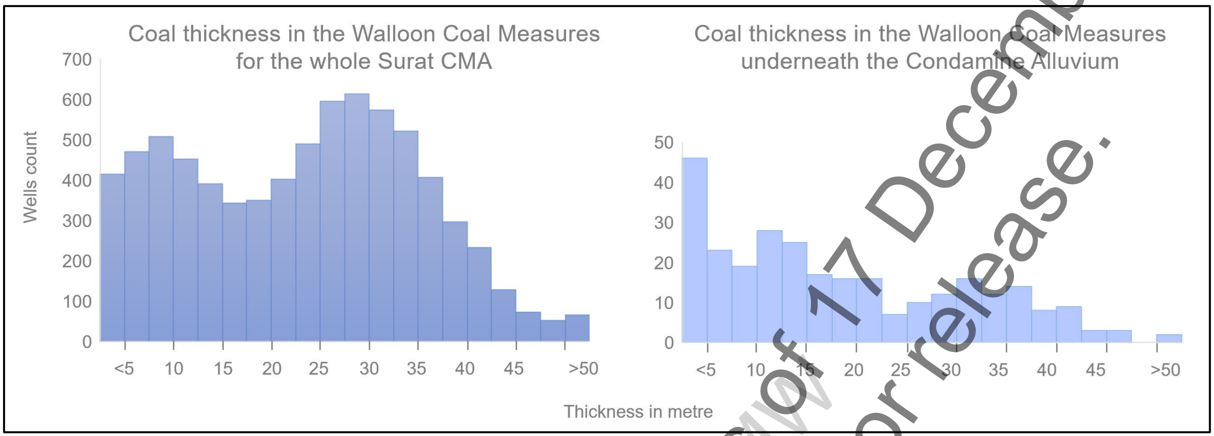

Figure 2-4: Distribution of coal thickness in the Walloon Coal Measures for a) the whole Surat CMA and b) the area underneath the Condamine Alluvium

2.5 Ground movement from non-CSG influences

Ground movement can also be caused by other factors, such as: shrinking or expansion of high-clay-content soils due to changes in moisture content; depressurisation resulting from groundwater use in aquifers overlying the target coal formation; and land management practices, such as irrigation, tillage and land contouring. CSG related subsidence is, therefore, only one potential component of ground movement.

Analysis of ground movement data by OGIA as described further in xxx, suggests that soil type and moisture content have a major influence on seasonal fluctuation in ground movement of up to +/- 25 mm within xxx m from each other.

There are also a number of international examples documenting the effect of groundwater extraction for water supplies in unconsolidated formations where metres of subsidence has occurred as a result of over-pumping and the unconsolidated nature of the material within which depressurisation occurs. These are well documented and compiled in a technical report prepared for the IESC (Commonwealth of Australia 2015).

However, importantly, in the context of the Condamine Alluvium, groundwater levels have remained relatively stable over the last decade or so since the commencement of CSG. Therefore, any subsidence related to groundwater use (non-CSG) would have already occurred in this area.

2.6 Subsidence from Coal mining

The subsidence due to the open cut coal mining can be either related to the groundwater extraction to facilitate the mining (dewatering of open pits and desaturation of surrounding coal seams), and/or the physical removal of material at depth. The impact of subsidence due to an extraction of groundwater is very slight compared with underground mining. Coal mining involves the construction of tunnels and longwalls along coal seams, creating voids (Commonwealth of Australia 2014). When these voids become too wide and can no longer be self-supporting, then overlying rocks can collapse into the void. A combination of collapsing roof strata into the void and some compaction of the load bearing coal seam strata can result in movement at the land surface. Coal mining subsidence impacts are site-specific and can be minimised by retaining pillars of coal to support the overlying strata, and/or grouting (infilling surface cracks) to some extent.

Subsidence due to withdrawals of fluids from the subsurface (in both CSG production and coal mining) is typically caused by elastic compaction (reversible) and is less than the effects from underground mining. OGIA observed (using InSAR data) around 90 mm of total ground movement within the gas fields since CSG production in 2015 (OGIA2021), gradually reducing at the margins of gas fields and no sign of subsidence further away from the gas fields. Comparatively, the maximum vertical subsidence occurring at the land surface from underground mining is typically irreversible and can be in the range of 1 to 2 m (Holla & Barclay 2000).

2.6.1 Subsidence vs change in slope

There have been limited studies on CSG-induced subsidence and its consequences on surface infrastructure and the environment (Wu, Jia & Wu 2019; Jayeoba 2020). In late 2020, OGIA engaged with landholders of cropping land in the western part of the Condamine Alluvium, seeking their understanding of potential consequences of subsidence on farming activity. While there were diverse perspectives expressed, there was consensus that rather than the overall magnitude of ground movement, the main concern would be change to the ground slope and aspect of the land resulting from variation in ground movement at the farm scale. Such change could potentially affect surface water drainage directions, which may have implications for irrigation and other farming practices.

The change in slope at a farm scale may result where differential ground movement occurs due to differences in magnitude of subsidence over time – such as in early phases of development when depressurisation propagates away from a well or gas fields, or along the margins of the gas fields where depressurisation tappers away with distance.

3 Monitoring methods and techniques

3.1 General

In relation to subsidence, monitoring of the ground surface is necessary to establish background conditions – such as the landform and slope – and to assess changes to the background conditions in response to natural, anthorpogenic and CSG-induced subsdience. For this reason, ground movement monitoring is necessary in areas away from CSG production, where subsidence would not be a component of ground movement. This data assists in understanding background movement unrelated to CSG depressurisation.

As discussed in earlier sections, there are two components to the assessment of subsidence. The first is the change in ground elevation or displacement. The second is the potential change in slope where there is differential ground movement at a farm scale. Through engagement with the community, the change in background slope is the metric of most concern and the focus of monitoring.

In this section, methods for determining spatial variations in slope at a farm scale are discussed and evaluated using the results from a farm scale pilot completed by OGIA in 2021. In addition, remote sensing data is presented to evaluate the temporal change in ground movement in relation to both CSG and non-CSG influences.

3.2 Monitoring change in slope (spatial variations)

3.2.1 Context

An understanding of background slope conditions and spatial variability is necessary to evaluate the potential for change from CSG-induced subsidence. This is because potential consequences at a farm scale will be dependent on both the magnitude of CSG-induced subsidence, and the background slope upon which any change is expressed - where a property has a minor slope, minor changes may have higher consequences.

To support the evaluate of background conditions and change, in collaboration with the community, OGIA has undertaken a property scale pilot to test the appropriateness several survey methods to establish slope at a farm scale. The objective of the project was also to guide the approach to be applied more broadly across the Surat CMA. Techniques were selected to evaluate the suitability of monitoring tools in relation to scale, repeatability and suitability for cropping lands.

3.2.2 Tools and techniques

A range of tools exist to monitor ground slope and motion at either a local or regional scale. Some methods measure relative change in elevation, while others are better at measuring absolute ground elevation. In the context of CSG-induced subsidence, important considerations for monitoring ground movement are: the accuracy of the measurement (millimetre accuracy when measuring changes over time); the need for minimal disturbance in and around the measurement points; and cost-effectiveness in data collection. A summary of techniques and methods is provided in Table 7 1.

Table 7-1: Methods for measuring ground movement

Method	Mode and frequency	Measured parameter	Density of data acquired	Suitability and practicality	Application in the Surat CMA
InSAR	Satellite based, every 6 days	Change in elevation	Data acquired every	☐ Measuring change over time (temporal monitoring) ☐ Not suitable for establishing a digital terrain model ☐ Some limitations in cultivated areas	☐ Multiple CSG tenure holders acquire and analyse this data in accordance with State and Commonwealth approvals.
Airborne LiDAR	Flight survey, when tasked	Absolute elevation	Typically 5 to 10 ground strikes per 1 x 1 m	☐ Establishing digital terrain model and slopes (spatial measurement) ☐ Not suitable for comparing absolute elevation from two different surveys at two different time periods ☐ Some limitations in heavily vegetated areas	☐ CSG tenure holders acquire for specific one-off project purposes. ☐ Arrow Energy periodically acquire for the assessment of subsidence.
Drone LiDAR	Above-surface survey, when tasked	Absolute elevation	Typically 40 to 50 ground strikes per 1 x 1 m	☐ Very similar to airborne LiDAR, but with higher density of data points ☐ More expensive than airborne LiDAR ☐ Some limitations in heavily vegetated areas	☐ Project specific data acquisition.
Terrestrial survey	Physical on-ground survey, when tasked	Absolute elevation	Typically every 25 x 25 m	☐ Similar to Drone LiDAR, but most expensive ☐ Some limitations in vegetative areas	☐ Farm scale surveys.
Geodetic network	Permenant survey marker	Absolute elevation	Typically one per 50 x 50 km	☐ High accuracy point dataset. ☐ Given frequency of capture and stand alone point distribution, less suitable for slope analysis.	☐ More than 140 points located across the Surat CMA installed by industry and Geoscience Australia.
RTK	Vehicle or machinery mouned ground survey	Absolute elevation	Typically every 25 x 25 m	☐ High accuracy low precision data collection. ☐ Suitable for slope analysis as high relative accuary. ☐ Local paddock scale data acquisition.	☐ Commonly acquired as part of routine farm activities – such as during planting, harvesting and spraying.

Notes
LiDAR = light detection and ranging, RTK = real-time kinematic global positioning system (GPS)

3.2.3 Challenges

As detailed in previous sections, a significant challenge for monitoring ground movement is that it may be caused by a range of environmental and anthropologic factors. Most of these influences are seasonal, such as variations in soil moisture profile resulting from variations in rainfall and farming activities. It is therefore impractical to use a single point-in-time measurement of a farm’s elevation and slope as a baseline. Instead, to eliminate seasonal effects, a baseline trend from data collected over a reasonable period is a more useful approach to establish CSG-induced subsidence.

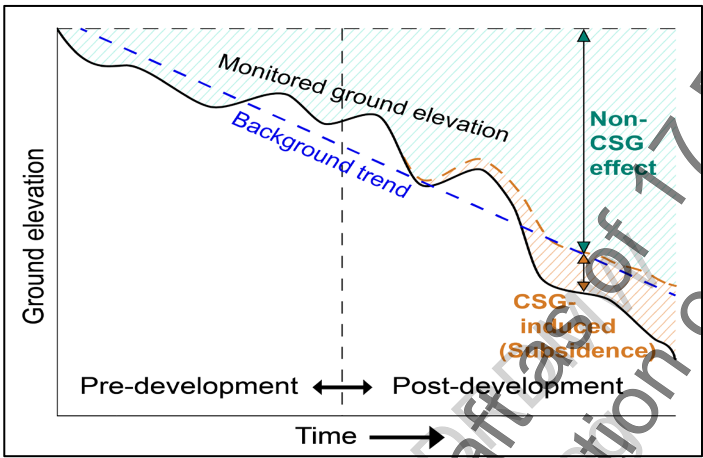

Figure 2-1: Schematic showing factors affecting trends in ground movement

In addition to the challenge associated with determining a CSG-induced ground motion signal, there are limitations with some monitoring tools, data availability and there appropriateness to be applied at a regional scale. These are summarised in

3.2.4 Property scale assessment

To support the evaluation of tools to establish background conditions at a property scale, OGIA designed a farms scale pilot and engaged a registered surveyor to lead the data collection. The objectives of the project were to:

- ☐ collect data using various monitoring tools;
- ☐ compare resulting products in terms of ground slope; and
- ☐ evaluate how the results compare with other available regional products.

The project site was a 700 hectare cropping enterprise located approximately 10 km south of Cecil Plains. The location was considered appropriate as it is located beyond the currently observed groundwater impacts from CSG and therefore no CSG-induced subsidence has occurred in this area.

The methods included in this study were remotely piloted aircraft system (RPAS) or drone acquired light detection and ranging (LiDAR), terrestrial ground survey (real-time kinematic (RTK) GPS), machinery mounted RTK and electromagnetic survey data for selected fields. In parallel, OGIA requested Airborne Laser Scanning (ALS) or fixed wing airborne LiDAR acquired by Arrow Energy for an area which includes the study location.

The data was collected in June 2021 and processed to produce a range of products including slope, aspect, digital elevation, and drainage. These products were then analysed by OGIA and compared with lower resolution datasets to analyse their appropriateness in establishing background conditions at the project site. For the ground survey, airborne and drone LiDAR datasets, each of the above-mentioned surfaces were generated in ArcGIS Pro using the following sequence of raster and vector toolsets:

- ☐ Fill raster – generates a hydrologically accurate surface by removing imperfections in a raster.
- ☐ Flow direction – calculates the direction of flow from every cell in an elevation raster.
- ☐ Flow accumulation – calculates the cumulative weight of cells flowing into downslope cells.
- ☐ Raster calculator – conditional statement to exclude flow accumulations of greater than 50.
- ☐ Stream order – assigns numeric order to stream networks based on the number of tributaries.
- ☐ Stream to feature – converts a raster linear network to a shapefile vector dataset.

Side by side images of drone and airborne LiDAR stream analysis? Could we also show the terrestrial gound survey data and the ATV data?

Observations from this analysis are summarised as follows:

- ☐ Terrestrial ground survey is labour intensive to collect, has a high absolute accuracy at the point of capture. However, in terms of the derived slope product and stream networkthe derived elecprovides insufficient detail to assess changes in slope or localised depressions….
- ☐ ATV….lower accuracy, lower data density….
- ☐ Drone…high density appropriate for
- ☐ Airbore…lower desity but similar drainiange pattern, efficient….
- ☐ Results thus far conclude that the surface drainage pattern across a paddock, derived from an aerial LiDAR survey, is the most suitable and cost-effective method to establish background slope, as it also helps in identifying minor slopes and depressions. As drone and airborne LiDAR show a similar drainage pattern, airborne LiDAR is therefore considered a cost-effective method for slope analysis and assessing changes over time at both a regional and property scale.
- ☐

Conclusions:

- ☐ Fixed wing airborne LiDAR is appropriate for establishing background conditions.
- ☐ For the purpose of generating a stream network analysis at the property scale, a high-resolution elevation surface is preferred as this can be down sampled as required. In comparison, low resolution (1 s and 9 s DEM) surfaces are suited to generating stream flow networks at a regional scale.

3.2.5 RTK timeseries analysis

The second study involved timeseries analysis of machinery mounted RTK technology. This data is commonly acquired in agriculture in large volumes across multiple years. While absolute elevation of a receiver varies between various machinery and mounting configurations, the relative change in derived slope between aquistins may be used to characterise background variability.

The site selected for this study is approximately 20 km west of Dalby, and about 5 km east of the nearest CSG well. RTK data from three collection vehicles was analysed for a 10-year period (Nov-2010 to Jan-2021) to produce rasters of elevation, derived slope and aspect surfaces. As multiple annual passes were conducted to produce this dataset, timesteps of digital elevation rasters were generated for individual passes or where multiple passes were required to complete spatial coverage.

A single land parcel measuring approximately 1,000 x 800 m was selected. Shed and housing areas were excluded as significant variability in elevation is observed, likely because RTK receivers require a period of calibration upon start-up of the machine. Measurements with a vertical and horizontal dilution of precision (DOP) of greater than X were also excluded to remove lower quality positioning data.

The data was processed at various resolutions········ to evaluate the app – 5 x 5 m, 10 x 10 m and 50 x 50 m.

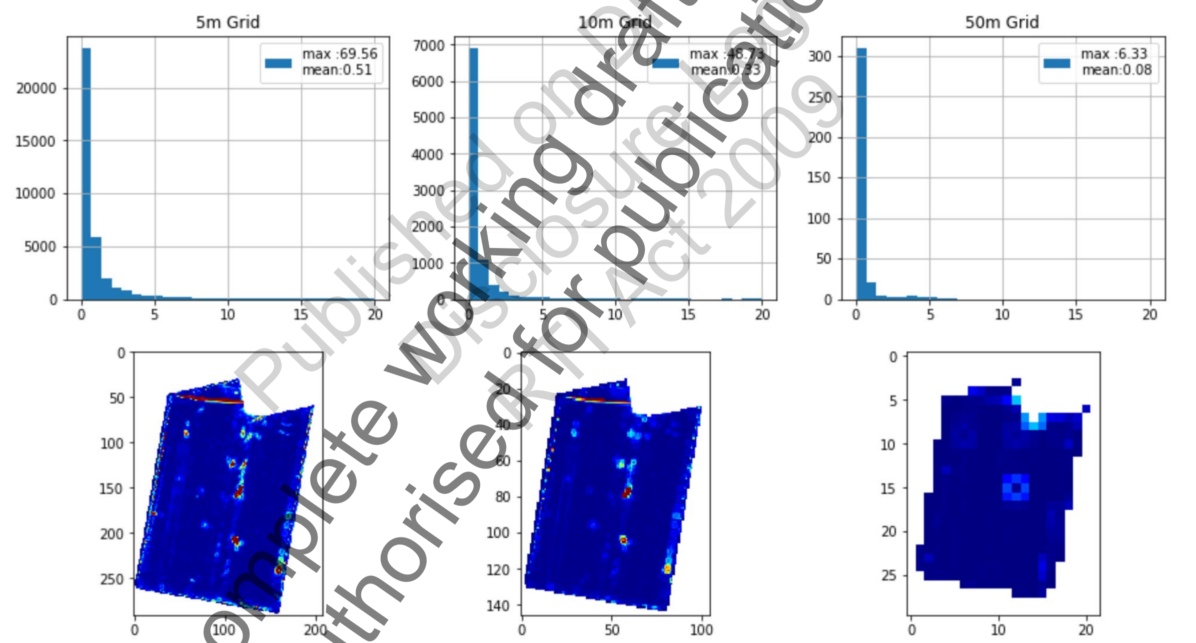

Figure 3-2 Variance in RTK derived slope at selected cell sizes

Observations from this analysis are summarised as follows:

- ☐ Results from this analysis indicate that the variance in slope change over a 10-year period decreases with increasing cell size (Figure 3-1). At a cell size of 5 m, derived slope is more representative of small-scale surface elevations which are subject to reworking by farm machinery. In comparison the derived slope is likely to be more representative of the land parcel topography at a cell size of 50 m.
- ☐ Terrestrial

3.3 Monitoring of rate of change in elevations (temporal variations)

3.3.1 Interferometric synthetic aperture radar (InSAR)

InSAR is a commonly applied and efficient technique whereby satellite-derived radar signals are processed to determine the change in ground elevation (i.e. ground movement). As shown in Table 3-2, there are three primary sources of satellite data available in eastern Surat CMA. These products vary in terms of their period of availblilty, resolution and frequency of data acquisition.

Table 3-2: Summary of available satellite data

Satellite	Advanced land observation satellite (ALOS)	Radarsat 2	Sentinel
Resolution	16.6 x 6.6 m	10 x 5 m	5 x 20 m
Frequency	46 days	24 days	12 days, 6 days from September 2017
Date range	2006 to 2011	2012 to 2017	2015 to 2021
Line-of-sight angle	34.9° - 39.2°	34.9 °	33.7 °

The raw satellite data must be processed to derive ground displacement from the first satellite capture. Data is commonly processed by private companies using proprietary algorithms and software to convert it into change in ground elevation. OGIA has directly secured the processed data for further analysis from a company called TRE Altamira.

Importantly, due to the angle of the satellite orbit data is collected at a line-of-sight angle. For the purposes of OGIA's assessment, this data has been converted to true vertical height. OGIA will continue to liaise with research organisations who are developing alternative algorithms to process available data.

3.3.2 Challenges

The InSAR technique requires processing of a large temporal dataset and maintencnce of consistent targets between data catpures.

This is often referred to the maintenance of coherence of between datasets. A key challenge with the processing of data is the loss of co

This means that ground movement over every 6 to 12 days is available – noting that not all data points can be converted to ground movement such as some heavily cultivated areas.

3.3.3 Analysis temporal trends

Figure 7-3 shows available point cloud around the eastern gas fields and along the western edge of the Condamine Alluvium. This figure shows ground movement over a period from early 2015 to mid-2021 as mm/year in different colours (red – higher downward ground movement; yellow – medium downward ground movement; green – neutral or upward ground movement). Charts of ground movement over time at representative locations with respect to proximity to gas fields are also shown as insets. For example, the insets in the bottom figure are from four locations around a CSG field. Moving from east to west, these are: away from the field, margins of the field, centre of the field and then again away from the field. At those locations ground movement is averaged from all data point within an area of about 250×250 m.

To demonstrate local-scale and natural variations in ground movement, similar data is also shown at a local scale at two different locations in and around the Condamine Alluvium – this time with and without averaging on the upper panel of Figure 7-3.

Some of the important observations are as follows:

- Total ground movement of up to about 90 mm is noted since 2015 within the gas fields (concentration of red points), which gradually reduces at the margins of gas fields (yellow points), changing to a nearly flat rate (green points) further away from the gas fields. This pattern of ground movement is attributed to CSG depressurisation.
- The rate of subsidence is higher in the early stages of development but will stabilise to near zero in the later years as shown in the long-term predictions (Appendix F) and described in later sections.
- Ground movement unrelated to CSG depressurisation and away from existing CSG development, both within and outside the Condamine Alluvium, suggests that the ground can frequently move up and down by around 25 mm/year and the ground movement can also vary significantly at a local scale (by up to 25 mm within 100 m). This is likely to be due to variations in soil type and associated changes in moisture content.
- Despite local variations in the rate of movement, the average trend from all data points within a local area shows a more consistent pattern of observed ground movement (Figure 7-3).
- Rising trends are observed in some eastern parts of the Condamine Alluvium with multi-year trends in ground movement which appear to correlate with rainfall pattern. This is likely due to overall moisture content that influences ground movement through drying and swelling of soil.
- Despite some limitations with InSAR data in cultivated areas, observed trends from the available data indicate ground movement within farms is highly variable, both spatially and temporally, apparently due to farming activities. Cultivated areas are therefore unsuitable for assessing changes in elevation, except in those parts of the farms that are less affected by these activities – such as near sheds, houses and other infrastructure.

3.3.4 Other influences on ground motion

Conceptually, there are a range of potential influences on the observed ground motion measured by InSAR. To understand the contribution of those influence on the observed signal, OGIA has begun to explore the application of machine learning models to extract further insights from the available monitoring data.

OGIA is has applied the random forest regression to develop subsidence prediction models from a range of input data including rainfall, soil types, nearby CSG water extraction, consumptive water use and parameters relating to the depth and thickness of coal. The model objective was to predict accumulative ground motion from 2015 at any location and to determine the importance of input data. The model was developed as a proof-of-concept in a small focus area – approximately 15 km².

The InSAR data was randomly divided in training (80%) and testing (20%) datasets. Both the training and testing models produced R^2 values of > 0.95, indicating a high level of agreement between the observation and predcited values. For the focus area, well water production and coal proportion were the most important input datasets to predictions. The model was not sensitive to soil type and clay percentage, but this most likely reflects the limited spatial extent and variability in those datasets in the proof-of-concept model area.

As more InSAR data is compiled by OGIA, it is anticipated that these models will provide some insights into the explanatory power of various parameters in the prediction of subsidence. This will also support the signal separation to derive CSG impact signals, which may be useful in groundwater model calibration.

4 Modelling of CSG-induced subsidence

4.1 Approach

Both analytical and numerical methods have been developed for the simulation of CSG induced subsidence, however, a comparison of both methods found that the prevailing challenge is in estimating the pressure distribution. It is difficult to account for complex 3D pressure distribution using analytical models, and so numerical models are more commonly applied (Wu et al. 2018).

While numerical models are often used for solving complex problems that involve heterogeneity and boundary conditions, significant run times are not uncommon due both to complexity and the iterative nature of the numerical solvers. Long run-times limit options for calibration/history matching and uncertainty analysis. As such, there are significant benefits in developing fast-running analytical models where it can be demonstrated that the analytical solution can approximate the numerical solution with acceptable accuracy.

As described above, one of the controlling factors for CSG induced subsidence is the pressure distribution within geological layers. OGIA has developed a regional groundwater model accompanied by an ensemble of 3,000 parameter sets to predict groundwater impacts from CSG development. Importantly, the regional model includes a representation of dual phase flow, and so, is able to provide estimates of the 3D pressure distribution in the system. As such the regional groundwater model has been used to provide the pressure conditions for geomechanical modelling thus addressing the first point above. The remaining challenges lie in the representation of geomechanical properties, calibration/history matching and the simulation of subsidence within an acceptable uncertainty framework.

To address these remaining challenges, OGIA has developed a 3D numerical geomechanical model and compared the results with an analytical solution to find a suitable degree of similarity between the two methods. This finding has subsequently led to the development of a history-matched ensemble of analytical models which have been used for predictions of CSG induced subsidence and changes in slope.

The following sections provide further detail on the modelling methods, results, and conclusions.

4.2 Numerical geomechanical model

A geomechanical model represents the mechanical rock properties of geological units and can be used to estimate reservoir compaction and surficial impacts resulting from changes in groundwater pressure. OGIA, in collaboration with Schlumberger, developed a numerical geomechanical model for the central and western Condamine Alluvium to support the predictions of subsidence from CSG development. This geomechanical model is underpinned by a regional geological model developed by OGIA, a calibrated 1D Mechanical Earth Model (MEM) developed by Schlumberger and pressure predictions from OGIA' s regional groundwater flow model. The numerical geomechanical model has been developed in collaboration with Schlumberger in Techlog and Petrel platforms and simulations are carried out in the VisageTM geomechanical simulator. Key components in the development of this model are outlined in subsequent sections.

4.2.1 Model domain and architecture

The model domain largely covers the Condamine Alluvium, including parts of the Condamine Alluvium where CSG impacts are predicted to occur in the underlying Walloon Coal Measures. The model covers an area of about 6,500 km², 50 km by 130 km, referred to as the area of interest (AOI) and represented by the blue outline in . The AOI of the 1D MEM is also shown in , represented by the orange outline.

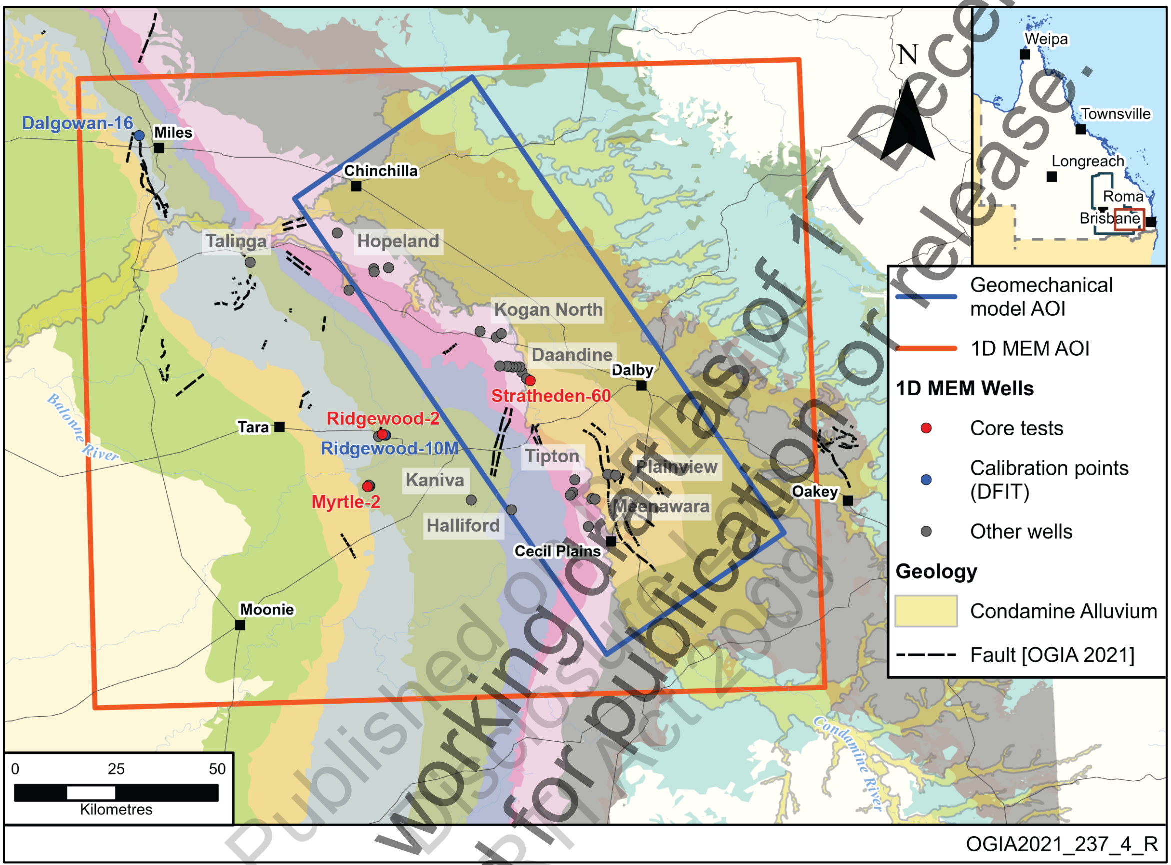

Figure 5-1 Domain for the 3D Geomechanical model

The architecture of the geomechanical model is based on OGIA’s regional geological model for the relevant hydrostratigraphic units – covering from ground surface to the base of the Durabilla Formation. Consistent with the groundwater flow model, the Walloon Coal Measures are sub-divided into the upper and lower Juandah, and Taroom coal measures. A total of 12 layers are used to differentiate between coal and interburden units in the Walloon Coal Measures. Some abstraction was applied to represent a single coal layer for each groundwater model layer (six in total), however, coal layer thicknesses were constrained by coal proportion maps derived from wireline logs, see Figure 5-2 .

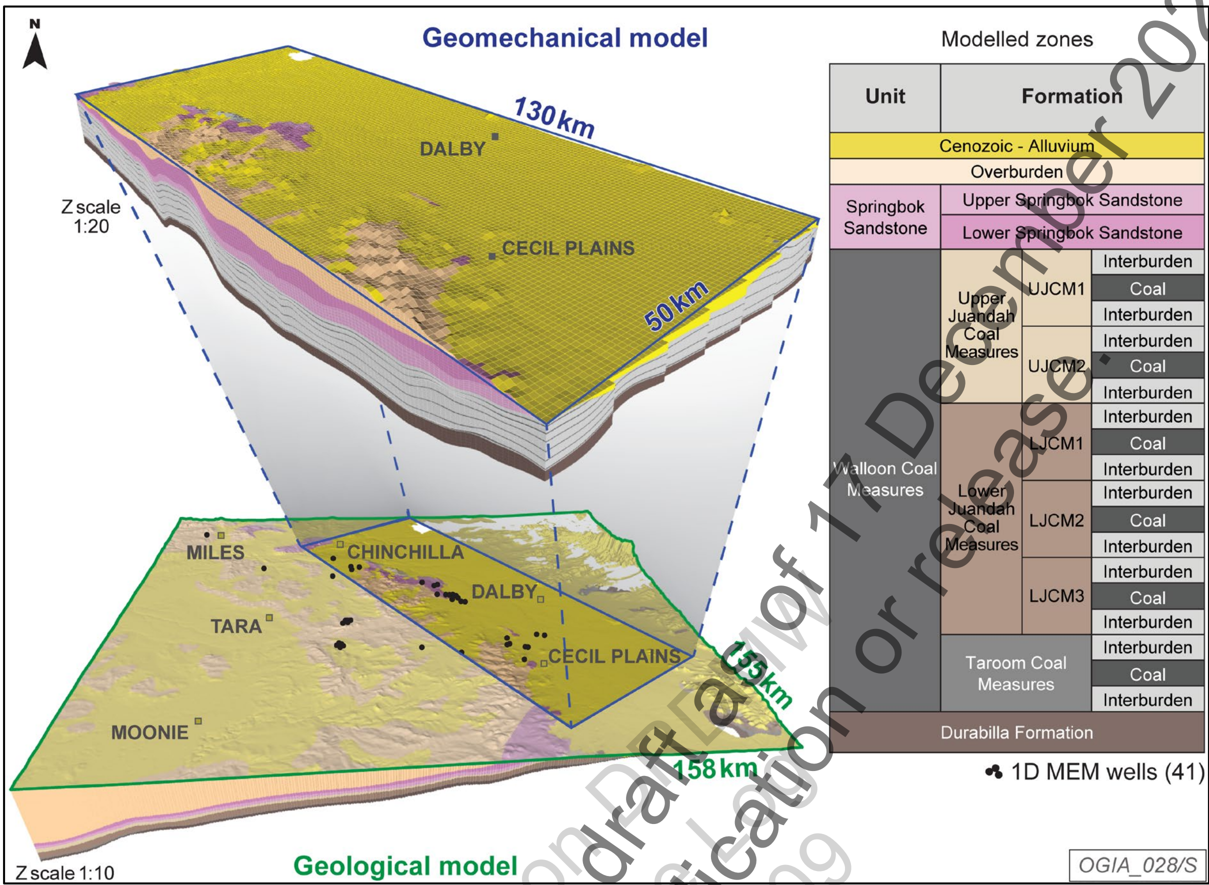

Figure 5-2 Geomechanical model architecture

The 3D numerical geomechanical model is constructed on a 750 x 750 m grid, with a total of 23 zones within the AOI, as shown in Table 5-1. To support numerical stability, the vertical grid resolution was further refined. The coal layers remained as one layers, most of the other layers were proportionally subdivided in relation with their relative thicknesses. The final vertical resolution of the static geomodel is 88 layers.

Additionally, several grid resolutions - vertical and horizontal - were considered and tested. The final model represents a fair trade-off between modelling objectives, accuracy, and computational demand.

Table 5-1 Geomechanical Model Layering

Architecture			Groundwater model		Geomechanical model		
Hydrostratigraphic unit	**Subdivision**	**Zone**	**Layer**	**Domain**	**Zone**	**Number of layers**	**Domain**
Cenozoic - Alluvium			1	Mobile	1	4	
Overburden			8	Mobile	2	8	
Springbok Sandstone	Upper Springbok Sst		9	Mobile	3	7	
	Lower Springbok Sst		10	Mobile	4	5	
Walloon Coal Measures	Upper Juandah Coal Measures	UJCM1	12	Immobile	5	4	Interburden
				Mobile	6	1	Coal
				Immobile	7	4	Interburden
		UJCM2	13	Immobile	8	3	Interburden
				Mobile	9	1	Coal
				Immobile	10	3	Interburden
	Lower Juandah Coal Measures	LJCM1	14	Immobile	11	6	Interburden
				Mobile	12	1	Coal
				Immobile	13	5	Interburden
		LJCM2	15	Immobile	14	6	Interburden
				Mobile	15	1	Coal
				Immobile	16	5	Interburden
		LJCM3	16	Immobile	17	6	Interburden
				Mobile	18	1	Coal
				Immobile	19	5	Interburden
	Taroom Coal Measures		17	Immobile	20	5	Interburden
				Mobile	21	1	Coal
				Immobile	22	1	Interburden
Durabilla Formation			18	Mobile	23	5	

4.2.2 1D Mechanical Earth Model

A 1D Mechanical Earth Model (1D MEM) has been constructed in Techlog (Schlumberger 2021).

The objectives of the 1D MEM are to define key geomechanical properties – Young's Modulus, Poisson's ration, Friction Angle, Unconfined Compressive Strength (UCS) as well as stress and strain parameters.

An initial data audit was undertaken to select 41 representative wells with relevant geophysical log suites (compressional and shear sonic slowness, density, calliper, porosity, GR, etc.), derived lithology and geomechanical properties. Five primary wells, with core tests and calibrations points, were used to define geomechanical transform and strain parameters (1D MEM developed in Techlog), and to model the remaining 36 wells, as shown in An initial data audit was undertaken to select 41 representative wells with relevant geophysical log suites (compressional and shear sonic slowness, density, calliper, porosity, GR etc.), derived lithology and geomechanical properties. From these 41 wells, three have core tests (MTXC) – Stratheden-60, Myrtle-2, and Rigewood-2, and two have calibration points (DFIT) – Ridgewood-10M and Dalgowan-16. These five wells are primary wells and defined relationships between log data and static mechanical parameters. Within the AOI, 25 wells were modelled using the calibration parameters of Stratheden-60 well and outside of the model area, the remaining 16 wells were modelled using the respective calibration (core data and stress measurements) from Ridgewood 2, 10M, Myrtle-2 and Dawogan-16 (see)The objective of a

1D MEM is to define geomechanical properties (Young's Modulus, Poisson's ration, Friction Angle, Unconfined Compressive Strength) along with strain parameters (e_x, e_y) and stresses for the 41 representative wells.

. This includes data, correlations and findings from four previous studies undertaken by Schlumberger (Myrtle field (SLB, 2010), Dalwogan-16 (SLB, 2010), Ridgewood field (SLB, 2010), Daandine and Stratheden fields (SLB, 2019)).

Several geotechnical reports were available from the Department of Transport and Main Roads, that recorded laboratory tests on the Condamine Alluvium sediments (generally taken near roads and bridges). Two reports on bridge foundations from the Department of Transport and Main Roads provided information on Unconfined Compressive Strength and Young's modulus (Queensland Government 2014 & 2012). Poisson ratios and Friction angles for the Alluvium were derived using Fakher, Cheshomi & Khamechiyan (2007) paper, as show in Table 2.

4.2.2.1 Overburden Stress

The overburden stress σ_V (or vertical stress) is caused by the weight of the overlying formations. Vertical stress was computed by integrating formation bulk density from surface to well total depth (TD) using the equation below.

$$\sigma_v = \int_0^z \rho_b(z) \cdot g \cdot dz$$

Where:

g is the acceleration due to gravity (9.81 m/s^2), ***z*** is depth and $\rho_b(z)$ is the formation bulk density as a function of depth and can be obtained from density log.

Whilst formation density can be obtained from wireline logs or from core density data, only bulk density logs were used in this study. Density over shallow sections up to seafloor was estimated using an extrapolated power law equation. A composite density log was constructed by splicing the extrapolated density and the original density to get a density profile from surface to well TD.

4.2.2.2 Rock Strength and elastic properties

To obtain calibrated rock properties for Poisson's Ratio (PR), Young's Modulus (E), Unconfined Compressive Strength (UCS) and Friction Angle (FANG), Multistage triaxial core test have been compiled for three key wells (Ridgewood-2, Myrtle-2 and Stratheden-60). Calibration was achieved through use of offsets and multipliers as outlined below:

For UCS, two components have been incorporated into the calibration, namely a lithology specific offset $loff$ and a formation multiplier Fm (this is done to reflect the variability associated with mechanical stratigraphy). For Young's Modulus and Friction Angle, a lithology specific multiplier was applied, while for Poisson's Ratio, an offset was used. Overall, a good match between calibration points and log is observed (see Figure 5-3).

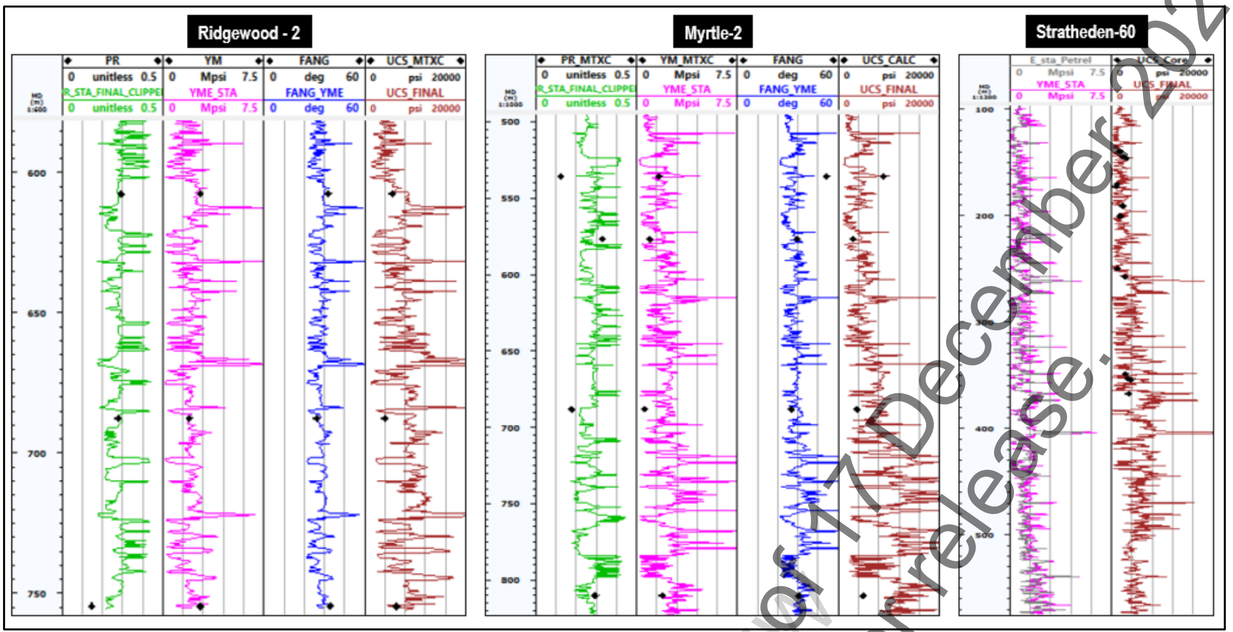

Figure 5-3 Calibrated rock strength and elastic properties for three wells (Techlog)

Several geotechnical reports were available from the Department of Transport and Main Roads, that recorded laboratory test on alluvium sediments along road and bridges (Queensland Government 2014 & 2012). These reports provided information on Unconfined Compressive Strength and Young's modulus property ranges. Using the extracted ranges of values, Poisson's ration and Friction angles were derived using Fakher, Cheshomi & Khamechiyan (2007), see Table 5-2.

Table 5-2 1D MEM elastic and rock strength properties

			Young Modulus (YME_STA_FINAL)				Poisson Ratio (PR_STA_FINAL)				Unconfined Compressive Strength (UCS_FINAL)				Frinction Angle (FANG_FINAL)			
			Mpsi				unitless				psi				degree			
Formation	**Zone**	**Lithology**	**Min**	**Max**	**Median**	**Std**	**Min**	**Max**	**Median**	**Std**	**Min**	**Max**	**Median**	**Std**	**Min**	**Max**	**Median**	**Std**
Condamine Alluvium*	1	Mixed	0.002	0.04	0.02		0.28	0.38	0.33		20	200	100		25	35	30	
Overburden	2	Mixed	0.17	7.01	0.76	0.46	0.17	0.38	0.29	0.03	371	15,071	1,842	993	26	54	29	1.8
Upper Springbok Sandstone	3	Mixed	0.15	6.66	1.08	0.60	0.17	0.43	0.29	0.03	383	14,726	2,508	1,303	25	56	30	2.7
Lower Springbok Sandstone	4	Mixed	0.07	7.86	1.07	0.81	0.17	0.45	0.25	0.04	102	17,313	2,556	1,761	25	61	31	3.7
Upper Juandah Coal Measures 1	5-7	Interburden	0.06	7.19	1.00	0.71	0.17	0.46	0.29	0.05	27	15,861	2,367	1,559	25	58	30	3.4
	6	Coal	0.08	1.24	0.25	0.10	0.24	0.48	0.43	0.03	46	3,308	1,196	223	25	30	26	0.5
Upper Juandah Coal Measures 2	8-10	Interburden	0.06	7.41	1.07	0.75	0.17	0.45	0.30	0.05	32	16,337	2,483	1,654	25	59	30	3.7
	9	Coal	0.08	1.53	0.27	0.15	0.22	0.48	0.43	0.04	263	3,985	1,237	338	25	31	26	0.7
Lower Juandah Coal Measures 1	11-13	Interburden	0.07	8.53	1.27	0.83	0.17	0.46	0.30	0.04	85	18,421	2,976	1,788	25	64	30	3.8
	12	Coal	0.09	1.81	0.29	0.23	0.17	0.49	0.42	0.04	136	4,602	1,273	501	25	32	26	1.0
Lower Juandah Coal Measures 2	14-16	Interburden	0.09	12.13	1.37	0.90	0.17	0.46	0.29	0.04	213	19,878	4,763	2,706	25	205	31	5.0
	15	Coal	0.09	1.60	0.29	0.19	0.19	0.48	0.42	0.04	292	5,658	1,911	624	25	36	26	1.0
Lower Juandah Coal Measures 3	17-19	Interburden	0.08	13.66	1.50	0.97	0.17	0.45	0.28	0.05	230	19,782	6,841	3,287	25	87	32	4.6
	18	Coal	0.10	1.80	0.29	0.17	0.17	0.47	0.42	0.04	262	9,016	2,569	753	25	32	26	0.7
Taroom Coal Measures	20-22	Interburden	0.09	8.72	1.47	0.93	0.17	0.48	0.28	0.04	248	19,866	6,690	3,443	25	65	31	4.3
	21	Coal	0.11	1.32	0.28	0.14	0.20	0.47	0.42	0.03	336	6,593	2,513	572	25	31	26	0.6
Durabilla Formation	23	Mixed	0.10	6.65	1.45	0.67	0.17	0.44	0.28	0.03	463	19,696	6,570	2,700	25	56	31	3.2

*(Queensland Government 2014, 2012; Fakher, Cheshomi & Khamechiyan 2007)

4.2.2.3 Horizontal stress direction and magnitude

Maximum horizontal stress direction results were extracted from image logs and from one MDT mini-frac. The maximal principal horizontal stress direction is consistently between N10° E to N20° E in the southern section of the AOI. Stress directions in the north seems to be different, at N75° E. However, stress directions in the north are only based on one well, Talinga-31.

The poroelastic horizontal strain model was used to calculate the horizontal stress ranges (minimum and maximum horizontal stress, σ_h & σ_H).

The two horizontal strains e_x and e_y may be compressional (i.e., for tectonic compression) or extensional (i.e., negative, to represent lateral spreading), and can be treated simply as calibration factors that can be adjusted to best-match the resulting stress estimates to any leak-off test data or specific modes of rock failure seen in image or caliper logs.

For this study S_{hmin} was calibrated with Diagnostic Fracture Injection Tests (DFIT) from Ridgewood-10M and Dalwogan-16. The maximum horizontal stress was estimated from an iterative process of matching the breakouts on the wellbore stability plot against the caliper log.

Horizontal strain parameters were subsequently applied as boundary condition to the geomechanical model at the σ_H & σ_h with e_y= 0.00057 and e_x = 0.00005 respectively.

A good match is observed between the calibration points (DFIT) and the modelled minimum horizontal stress. A reasonable estimate of the maximum horizontal stress is obtained from breakout observation against calipers logs.

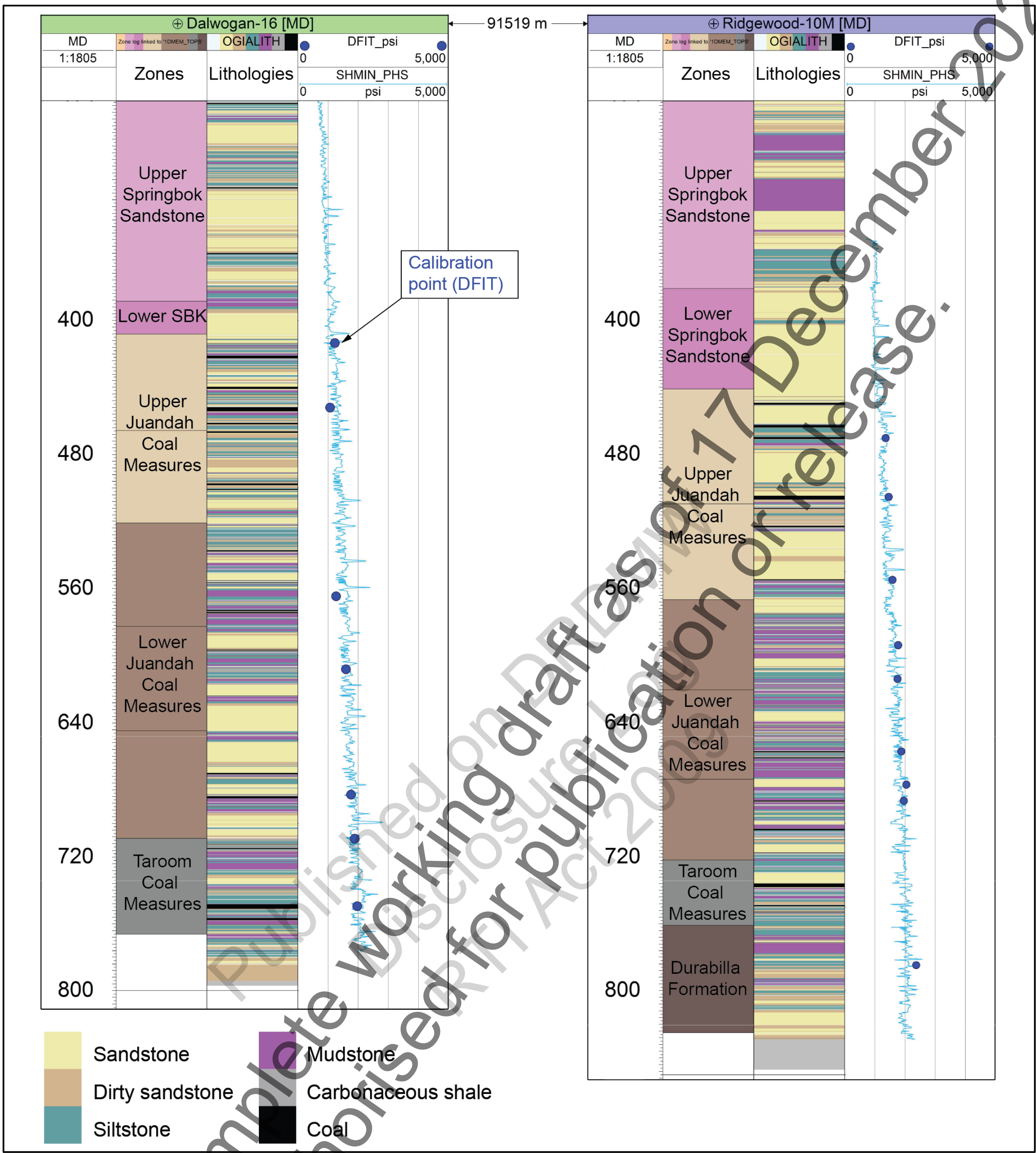

Figure 5-4 Horizontal stress vs DFIT calibration in Ridgewood-10M and Dalwogan-16

4.2.3 3D Mechanical Earth Model

The 3D MEM or geomechanical model incorporates both elastic and plastic properties derived from the 1D MEM together with the simulated pore pressure from the regional groundwater flow model.

4.2.3.1 Embedment and materials

The geomechanical model consists of the original geological model with the addition of side-burden, and under-burden. The geological model domain is represented using elasto-plastic properties required for the Mohr Coulomb model. The geological model domain is then surrounded by side-burden and under-burden which is represented with elastic properties only to capture loading effects

(See Figure 4-5). The embedded grid is aligned to the regional average SH_{max} direction (N15˚E) as identified by the 1D MEM study.

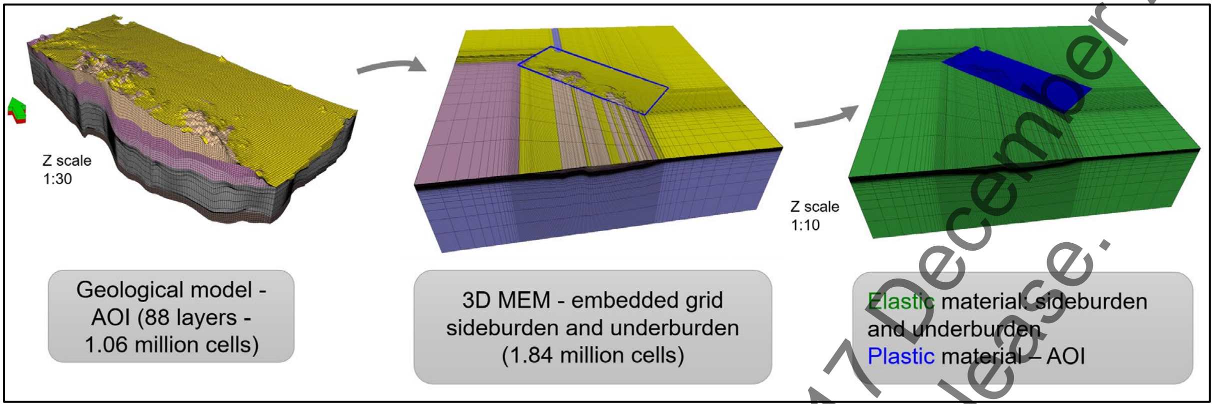

Figure 5-5 3D MEM embedment and materials

4.2.3.2 Property Modelling

Elastic and Plastic material properties derived from the 1D MEM (see section 5.2.2) have been interpolated into the geomechanical 3D grid using petrophysical modelling (Petrel).

The properties required to define elastic materials are density, Young's modulus, Poisson's ratio and Biot's coefficient (set as 1). To capture the plastic rock properties, additional fields are generated for: Unconfined Compressive Strength (UCS), Tensile Strength (TSTR)[1] as well as the friction and dilation angles.

The geomechanical model layering (see section 5.2.1) includes a representation of coal and interburden in the Walloon Coal Measures (lumping the total coal thickness in each zone into a single coal layer surrounded by interburden layers), as such, the population of geomechanical properties required some processing to produce commensurate properties.

For each zone, geostatistical analysis was run on 1D MEM properties to define appropriate variograms - a range of 20km was set for non-coal and 5km for coal zones. Figure 5-6 shows the coal thickness variograms for each of the sub-units the Walloon Coal Measures. Gaussian Random Function Simulation algorithm was used for interpolation of the geomechanical properties, based on an average property value for coal and non-coal at the well location (upscaling) and distribution functions (from all 41 offset wells) that retained the well logs spatial variability through each zone.

[1] Note: Tensile strength is defined as 10% of the UCS property and the dilatation angle is defined as 50% of the friction angle.

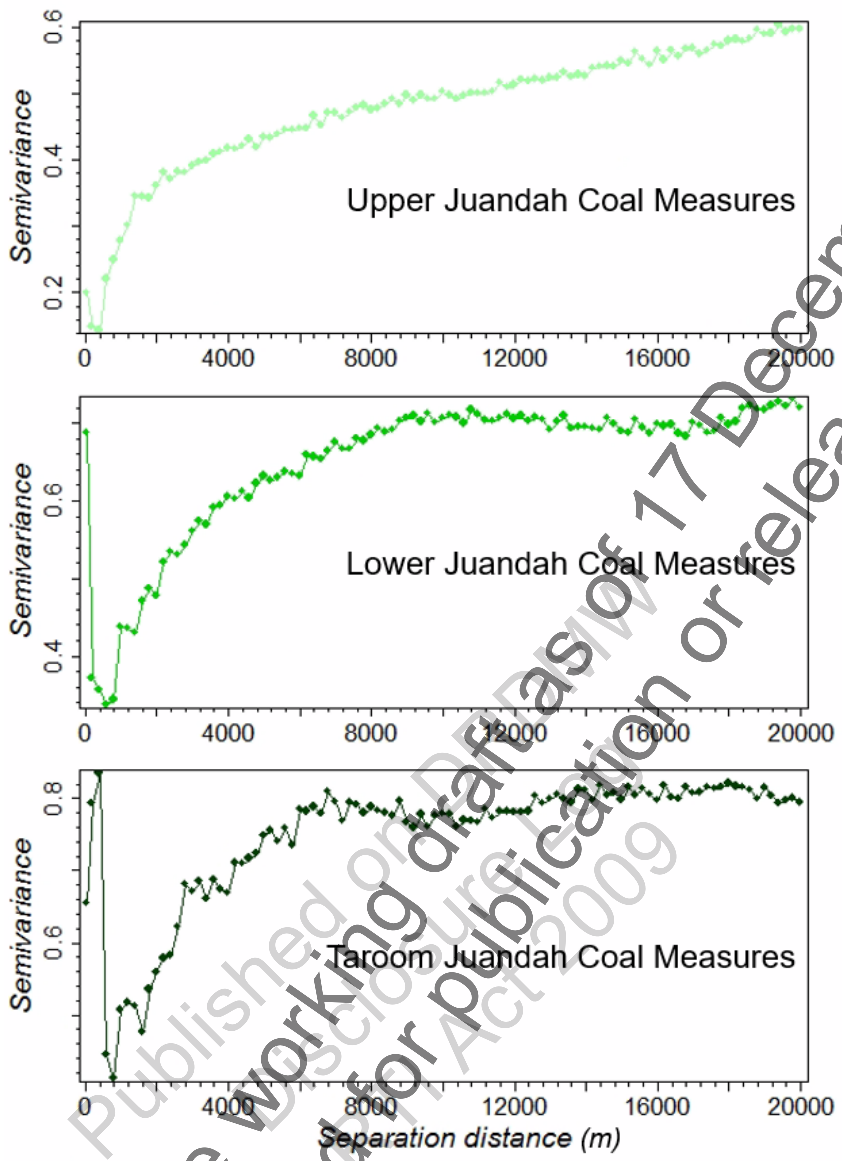

Figure 5-6 Semi-variograms for sub-units in the Walloon Coal Measures

4.2.4 Integration with the Regional Groundwater model

Pressure predictions from OGIA's groundwater flow model were extracted for all model layers for 12 time-steps – 1995, 2015, 2017, 2020, 2022, 2024, 2030, 2040, 2060, 2075, 2099, 2109. Heads from the model were converted to pressure gradient (psi/m) and pressure was subsequently calculated for commensurate geomechanical model layers based on their depth and the pressure gradient, see Figure 5-7. For each time step, pressures were extracted for two scenarios, a no development scenario, representing pressures as though no development had ever occurred, and a development scenario, representing all historic and planned CSG activities. Pressures were propagated into the model grid as properties which are used in the simulation stage. To assist with the development of this model, pressures have been derived from the best calibrated groundwater model or 'base' model from OGIA's calibrated model ensembles.

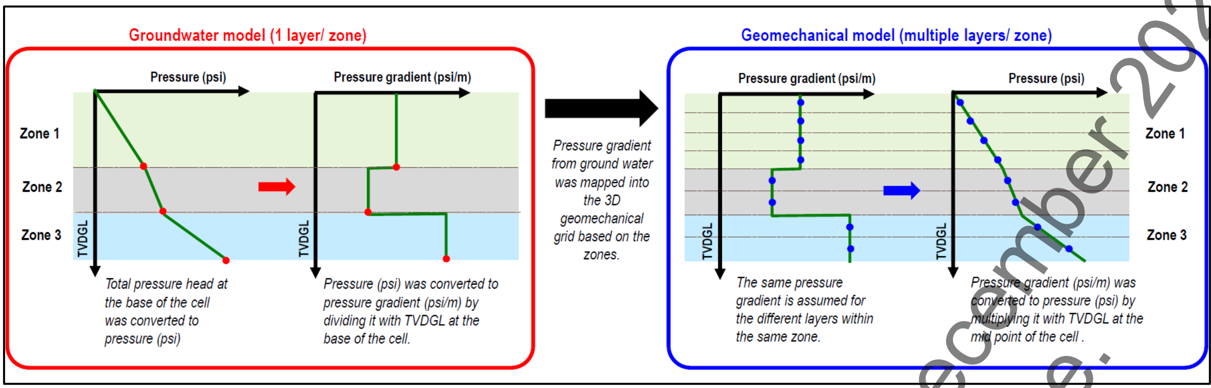

Figure 5-7 Conversion of groundwater heads to pressure

4.2.5 Subsidence Simulation

The geomechanical model was ported to the Visage geomechanical simulator and has been run with four randomly generated property realisations to assess the sensitivity of the model result to the rock property distribution (property fields were generated using the method outlined above, conditioned to 41 wells). The model produces vertical displacement at the surface as well as compaction for each unit for all scenarios for all of the above mentioned timesteps. Figure 5-8 presents the predictions for a single realisation for select timesteps.

The model has been run with multiple scenarios to test the influence of different stressors on subsidence. As such, the numerical subsidence model has been run with pressure inputs from the following groundwater model scenarios:

1. No-CSG scenario (accounting for consumptive water use only)
2. A CSG scenario (accounting for consumptive water use and CSG extraction

A series of sensitivity runs have also been conducted for both scenarios using a range of conditioned parameter fields and result are shown in Appendix 1.1. The key finding from this is that consumptive water use is not predicted to contribute substantially to the overall subsidence. Rather CSG depressurisation is likely to be the main contributor[2].

Once both of these scenarios have been run, the potential CSG contribution to subsidence is obtained by through the differential subsidence between 2 and 1 (an example for a single run is shown in Figure 5-8) [3] .

The maximum predicted CSG induced subsidence from this model is around 200 mm and occurs around the year 2060, after which rate of subsidence decreases and eventually flattens out. The model also suggests that the largest component of subsidence is due to coal compaction in the Lower Juandah Coal Measures (See Figure 5-9)

[2] The current modelling does not take into account poroelastic effects in the Condamine Alluvium which may be relevant in the context of unconsolidated material. However, it is not clear what materiality this may have for subsidence predictions. Future research by OGIA is expected to explore these effects.

[3] A separate differential scenario using pressure differences derived from 2-1 as an input to the geomechanical model has also been run and results are identical, suggesting a strong linear-elastic influence in the numerical model.

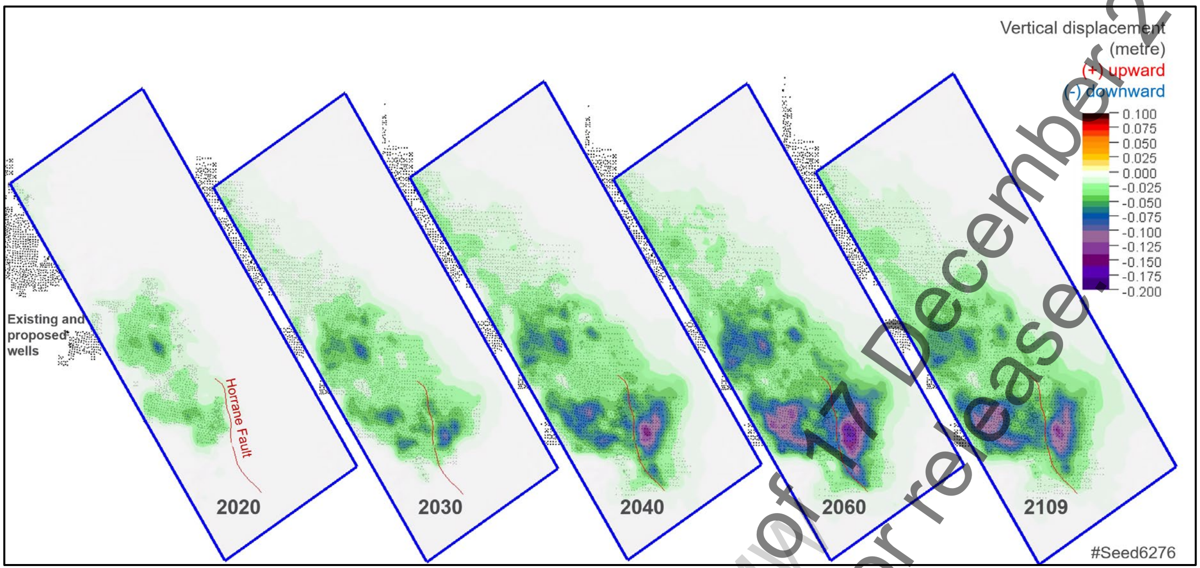

Figure 5-8 Vertical displacement at surface over time

Figure 5-9 Compaction for each of the main stratigraphic unit

4.2.6 Hypothesis Testing

As mentioned previously, several Indicators suggested that Subsidence in the AOI is largely controlled by linear-elastic processes and primarily by compaction (with no indicators of overburden arching).

To test this further, the numerical model was run first using a linear-elastic model only and then with a full Elasto-plastic model. the results are compared in Figure 5-9 below, showing a good correlation of 0.99 between the two predictions scattered around the 1:1 line. This confirms that CSG induced subsidence in the AOI is largely controlled by linear elastic processes (under the modelled pressure scenarios and the tested geomechanical property ranges).

Additionally, to test the hypothesis that coal compaction is largely realised at the surface, compaction from each layer was accumulated and compared to the modelled subsidence. Minimal overburden arching was observed as the total modelled compaction closely approximates modelled subsidence at the surface (see Figure 5-11).

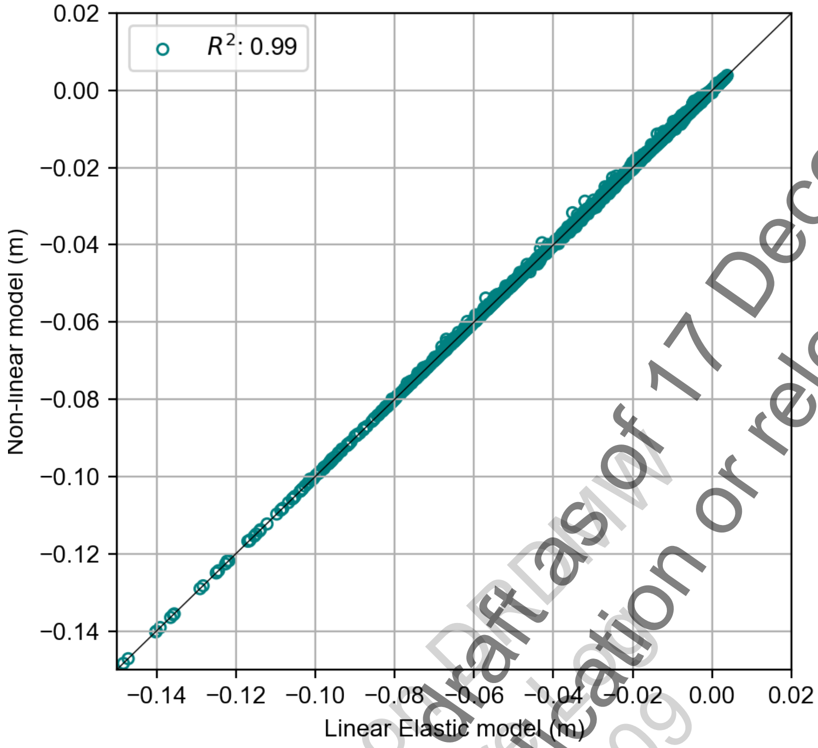

Figure 5-10 Non-linear vs Linear Elastic model predictions

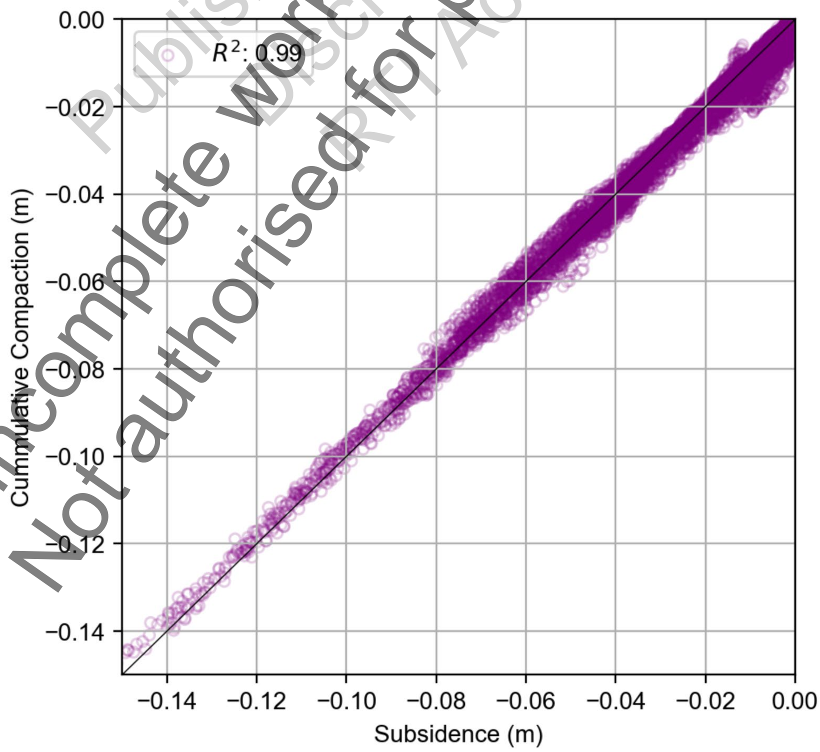

Figure 5-11 Cumulative Compaction vs Subsidence predictions

4.3 Analytical Subsidence model

As discussed in the section above, numerical modelling result reveal two key findings that provide opportunities for the development and adoption of simplified models, these are:

1) deformation processes in the AOI are likely to remain in the linear elastic regime; and
2) subsidence is likely to reflect reservoir compaction, as no overburden arching effect is predicted to occur.

As such, OGIA has developed an analytical model to predict subsidence accounting for uniaxial compaction. The model has been derived from (Settari 2002 & Fjaer 1992) such that:

$$\Delta H = C_m H \Delta P$$

Where ΔH is the change in thickness, H is the original thickness, ΔP is the change in pressure and C_m is the uniaxial compaction coefficient which is further defined by:

$$C_m = \frac{C_b}{3}\left(\frac{1+v}{1-v}\right)\left(1 - \frac{C_r}{C_b}\right)$$

Where E is the Young' s Modulus, v is Poisson' s ratio, C_r is the grain compressibility and C_b is the bulk compressibility

$$C_b = \frac{3(1-2v)}{E}$$

Assuming the ratio of $C_r \ to \ C_b$ approaches 0, the calculation for compaction can be simplified to:

$$\Delta H = \frac{(1-2v)(1+v)}{E(1-v)} H \Delta P$$

The above calculation assumes that compaction is primarily due to linear elastic processes and does not account for plastic deformation or the arching effect of overburden

The analytical model utilises the same layer structure as that of the numerical model.

4.3.1 Comparison with Numerical Model results

The analytical model was applied to the same layers as the numerical model using identical pressure and property fields to explore the ability for the analytical model to replicate results from the numerical model. A comparison of modelled subsidence from both models shows the two models are highly correlated with 98% of the variably in the numerical model captured by the analytical model. There are however, some differences at the larger displacements where the analytical model has a tendency to predict more subsidence compares to the numerical model. However, the analytical model provides a reasonable approximation of subsidence, and therefore, its use is considered appropriate for obtaining subsidence predictions, particularly if history matching/calibration is undertaken to ensure the model is able to explain historical observations.

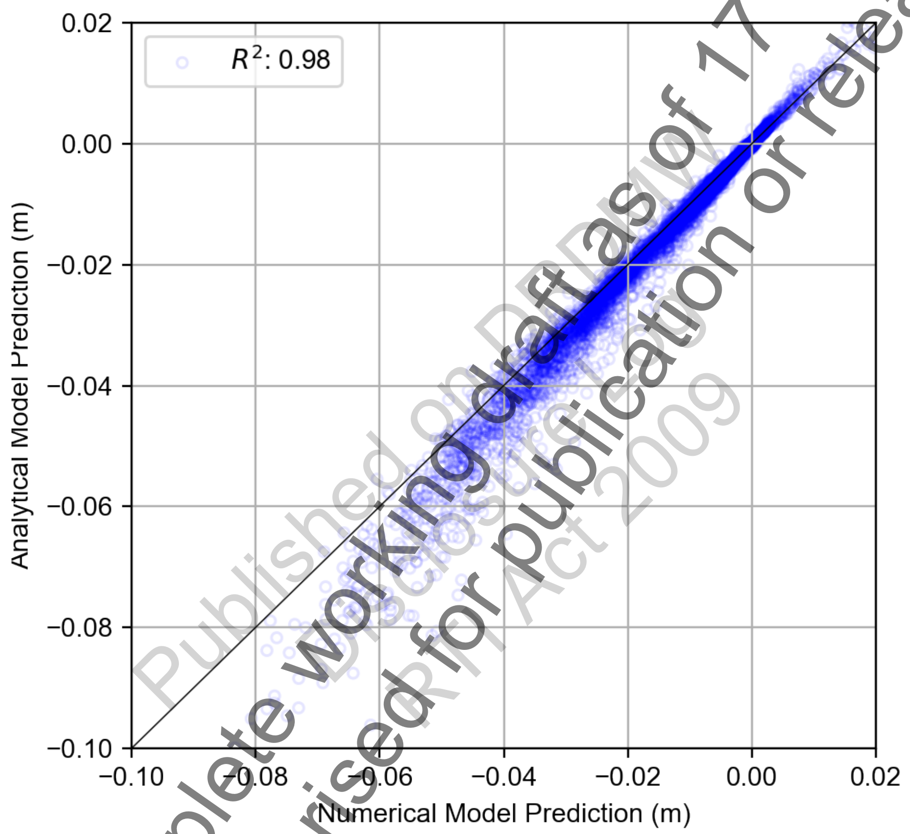

Figure 5-12 Comparison of predictions between Numerical and Analytical geomechanical models

4.3.2 History Matching

To underpin the history matching process, 1,000 stochastic parameter sets were generated for the entire Surat CMA. For each layer, corresponding parameter fields were generated for Young’s modulus and Poisson’s ratio.

4.3.2.1 Parameterisation

Each parameter field was generated using conditioned random gaussian simulations. Simulations were constrained by calculated parameters in the corresponding layer at each of the 41 wells described in X. Parameter distributions were drawn from the observed ranges presented in Table X and an additional random variance between +/-10% was assigned as to allow for some variability at the observations. A variogram range of 5 km was assigned for coal and 20 km for interburden. Stochastic parameter fields were generated using the GSTools Library developed for Python (Muller & Schuler n.d.)

Example parameter fields are shown below for the Taroom Coal Layer:

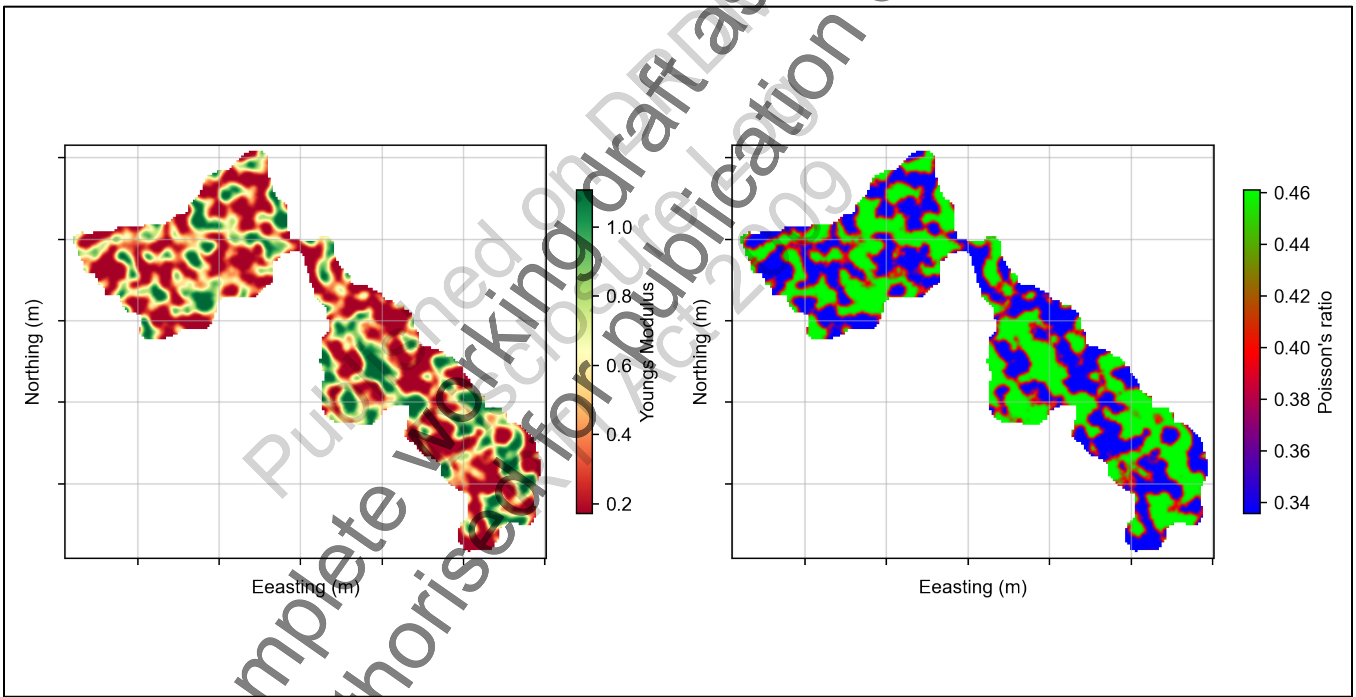

Figure 5-13 Young’s Modulus and Poisson’s ratio for a single realisation of the analytical compaction model

4.3.2.2 Observations

Seventy-two (72) observation targets were manually selected from InSAR data to constrain the subsidence model. The spatial distribution of these points is shown in Figure 5-13. These observation points targeted a cross section of signals including: within historical CSG development areas; at the fringe of active CSG development; and at the periphery where no CSG induced subsidence is observed. Signals which are thought to reflect natural process were not included in the observation dataset, as the compaction model is not designed to replicate these processes, but rather to explore potential CSG induced impacts only. To minimize the influence of noise in the history matching process, all InSAR points within a defined radius of representative observations (100-750 m) were averaged to produce a single representative timeseries for history matching.

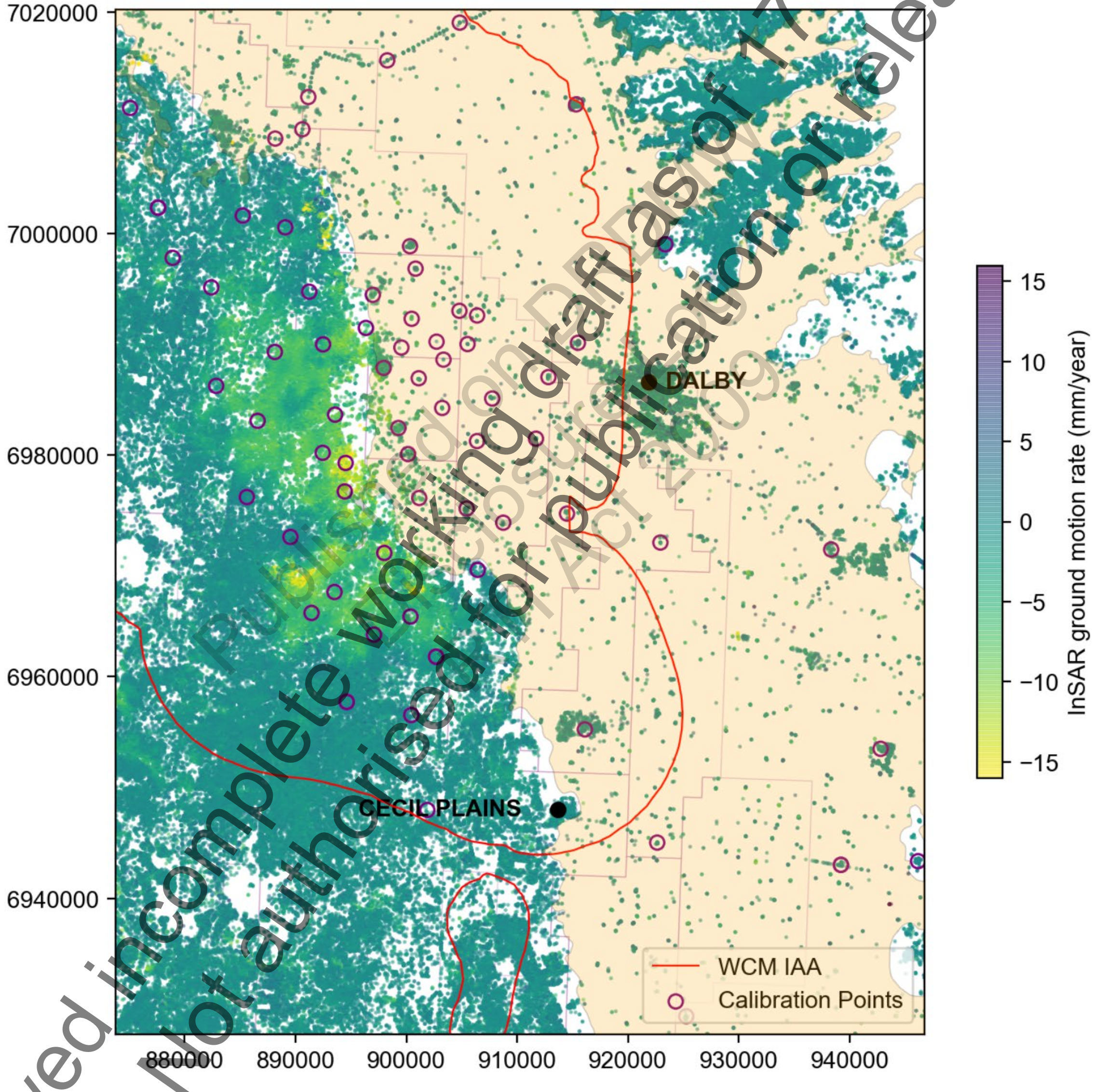

Figure 5-14 Map of Calibration points used for history matching

4.3.2.3 Rejection Sampling

Once all 1,000 models were run, a fit was calculated for each model by comparing the modelled vs observed rate of decline for two periods, pre- and post-CSG development. The transition date for these two periods is defined by the first date preceding more than three months of CSG production from any well within 10 km of the observation point. A root weighted sum of squared errors (RWSSE) was calculated for each realisation, such that, weighting was based on the rate of decline in the period, and so, was biased towards those observations which showed greater downward motion:

$$RWSSE = \sqrt{\sum_{i=0}^{n} nw_i \cdot (\hat{y} - y)^2}$$

Where the normalised observation weight $nw_i = \frac{w_i}{\sum_{i=0}^{n} w_i}$ and $w_i = \begin{cases} y, & y < 0 \\ 0, & y > 0 \end{cases}$, such that the weight is proportional to the rate of ground motion at each respective observation.

Figure 5-14 shows the $RWSSE$ for 1,000 ensembles. The top 50 models were subsequently selected to perform predictions. The performance of the selected ensembles ranged from 3.4 to 4.2 RWSSE.

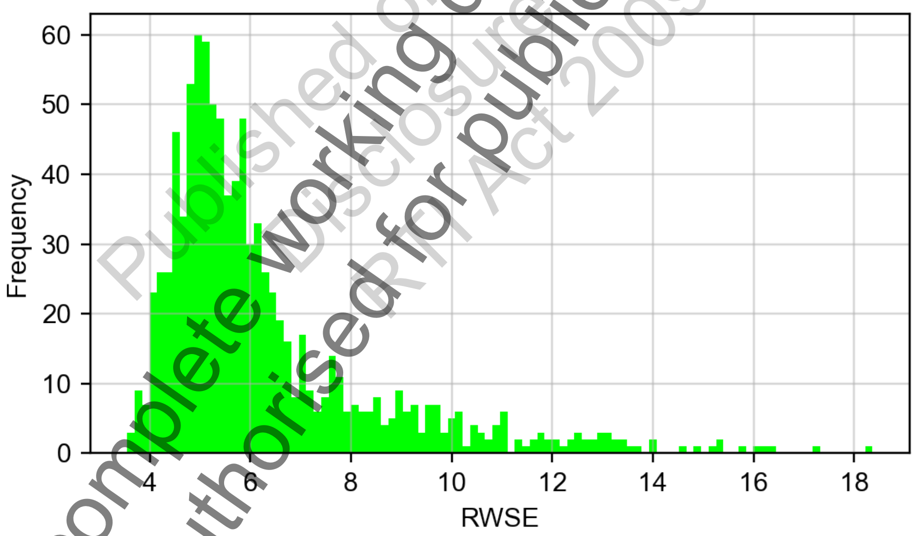

Figure 5-15 Distribution of model performance for 1000 parameter and observation ensembles

Examples of observed vs modelled subsidence are shown in the below figures for points within, nearby and distant to current CSG development.

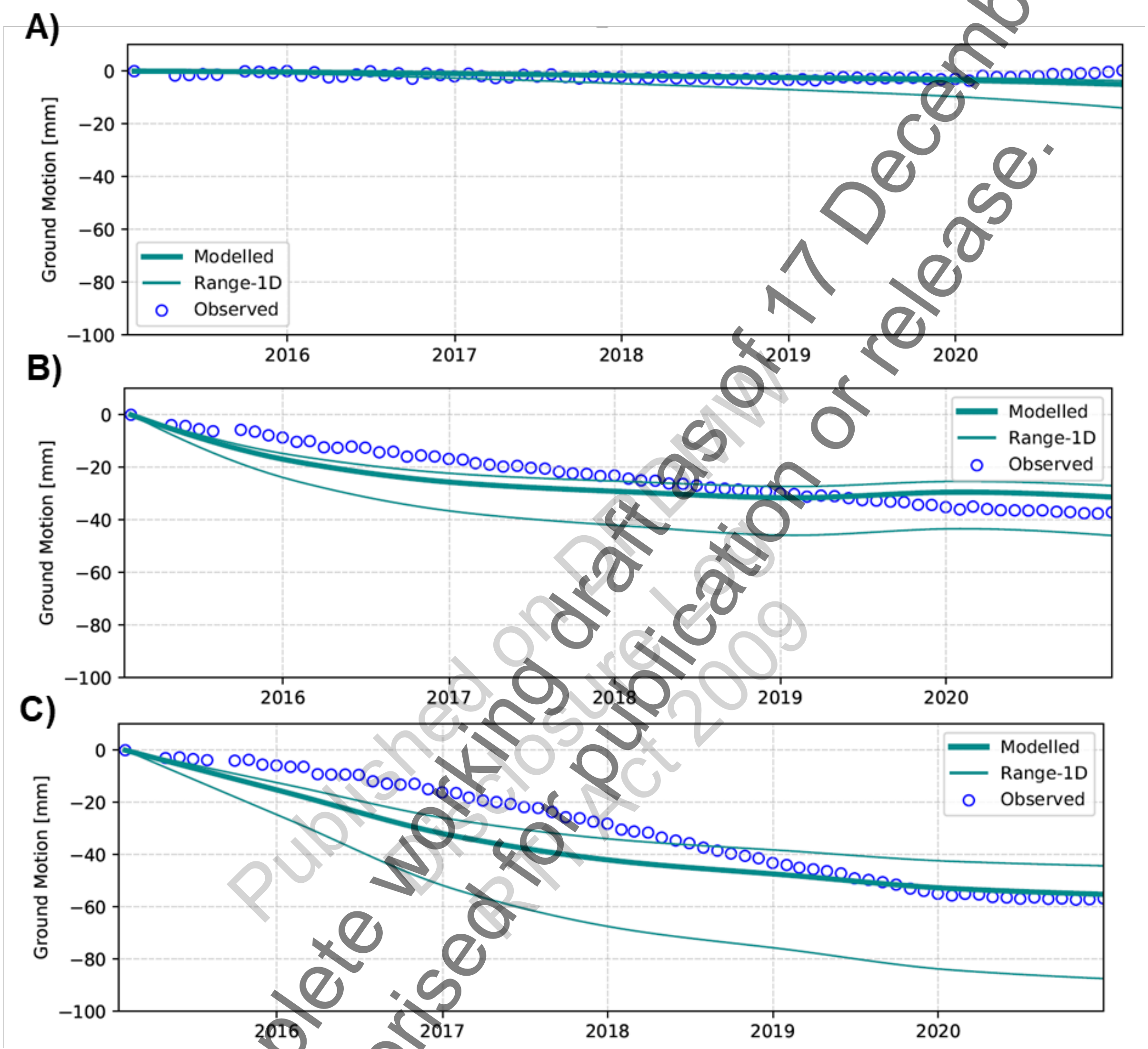

Figure 5-16 Observed and Modelled subsidence for A) Distant to active CSG, B) Nearby CSG Area and C) within a CSG development Area

Once selected, the 50 selected parameter sets represent a set of calibrated geomechanical fields. Figure 5-16 below shows an example for the mean and standard deviation of the calibrated parameter fields. The 50 parameter sets were subsequently retained for making stochastic subsidence predictions as outlined in the following section.

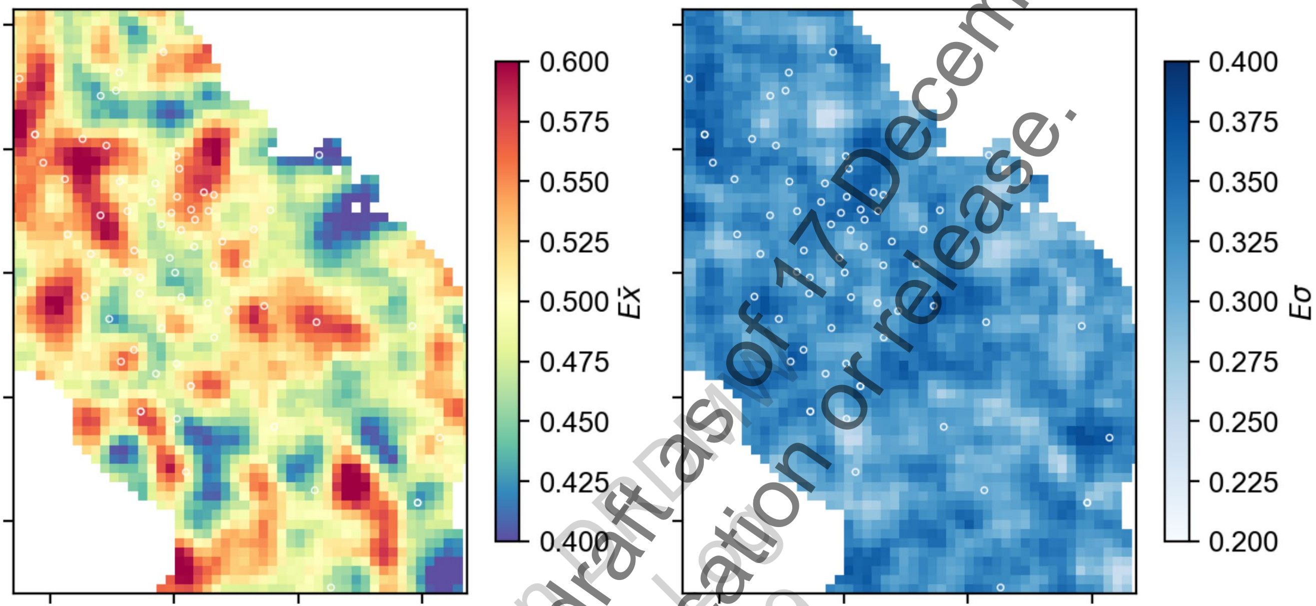

Figure 5-17 Map of mean and standard deviation for calibrated coal Young's Modulus in the Taroom Coal Measures

4.3.3 Predictions of subsidence

Subsidence predictions have been made for 1995, 2015, 2017, 2020, 2022, 2024, 2030, 2040, 2060, 2075, 2099 and 2109. Additionally, the maximum all time subsidence has also been calculated for each model cell for each of the 50 models used for predictions. The 50th percentile (P50) for maximum all time subsidence is presented in the UWIR and can be found in Appendix 1.3, together with the predicted year of maximum all time subsidence. Additionally, the probability of experiencing subsidence of up to 50mm, 100mm,150mm and 200mm has been extracted from those realisations selected in the rejection sampling process in order to represent the uncertainties associated with selected subsidence thresholds. These are presented in Figure 5-19.

Based on the modelling undertaken by OGIA, very few areas are likely to experience more than 200 mm of subsidence, with probabilities of 10-20% in some areas and up to 50% in a future development area near the Horrane Fault. This is likely a reflection of drawdown in the Walloon Coal Measures propagating against the fault, due to the reduced horizontal hydraulic conductivity across the fault zone. The spatial distribution of predicted subsidence closely mirrors the predicted patterns of depressurisation (see Appendix F of UWIR 2021). From a regional perspective, 97% of impacted areas (>10 mm in the long term) are likely to experience less than 100 mm of subsidence in the long term, see Figure 5-17, below.

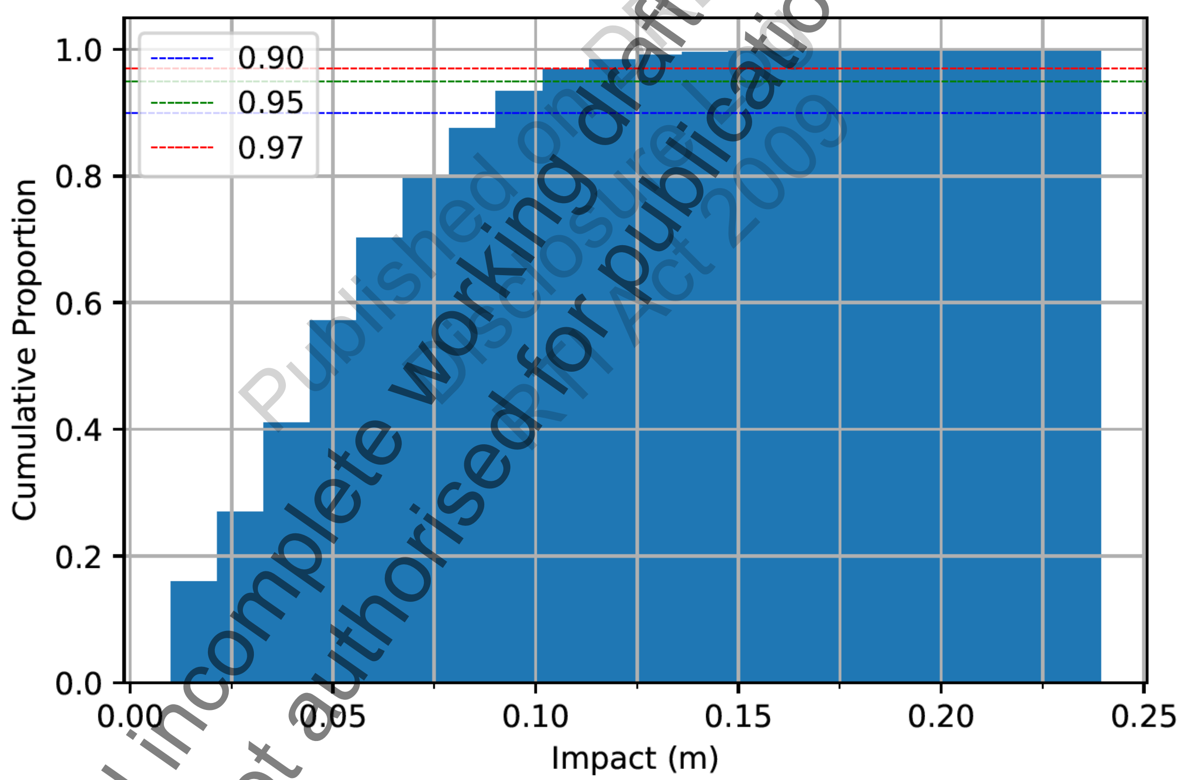

Figure 5-18 P50 Cumulative frequency of maximum predicted subsidence for affected areas (> 10 mm of predicted subsidence)

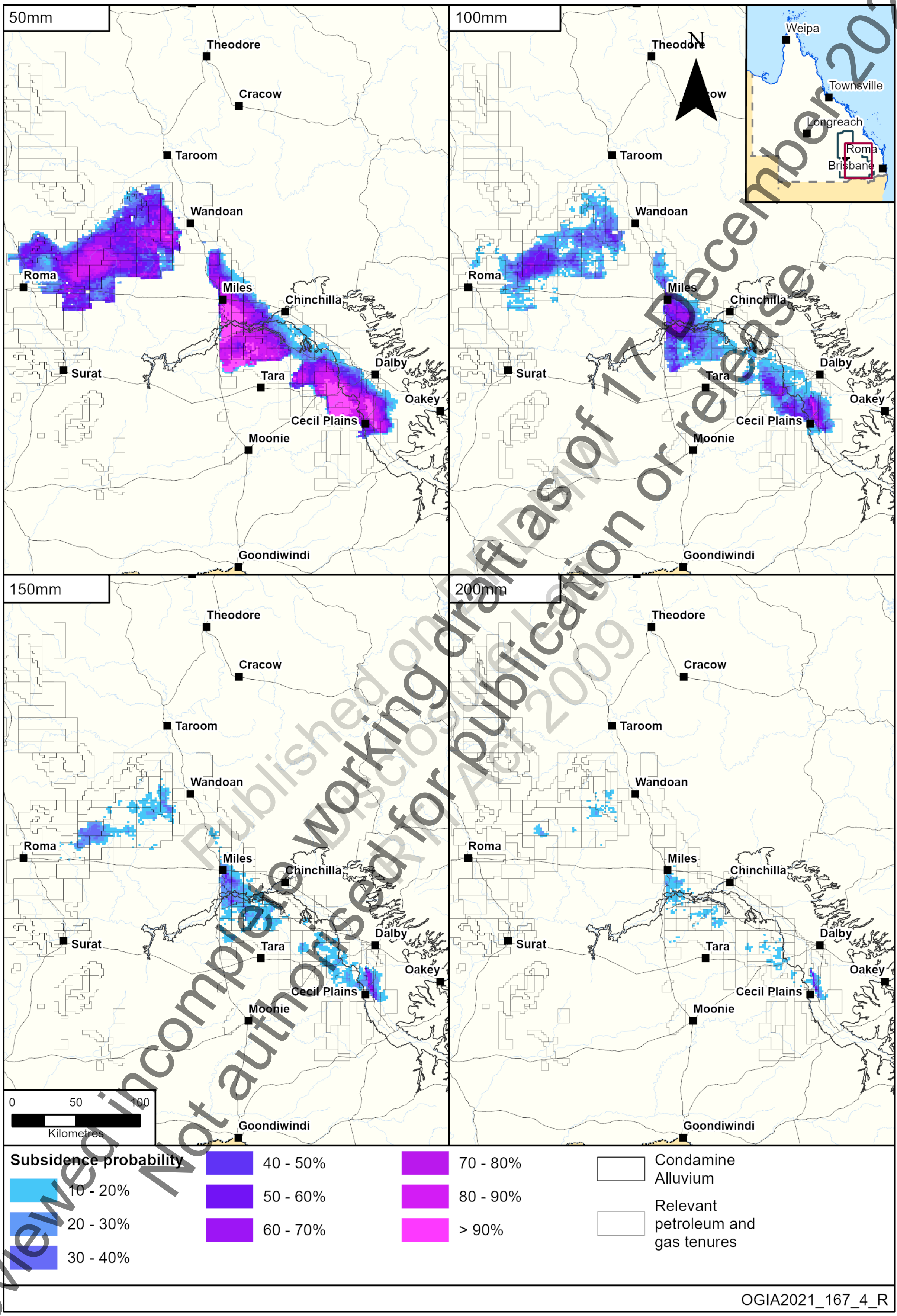

Figure 5-19 Predicted probability of realising subsidence greater than a) 50 mm, b) 100 mm, c) 150 mm and d) 200 mm

4.3.4 Predictions of change in slope

To estimate a change in elevation and slope associated with CSG development, the initial slope is first derived from a 9-second digital elevation model (DEM, 2000)[4].Slope is calculated using the gdaldem toolkit in Python (GDAL/OGR 2021).The method is derived from Horns formula (Horn 1981).

Future slopes are subsequently calculated based on a modelled ground surface for each timestep (obtained by subtracting modelled subsidence from the initial DEM). By subtracting all future slopes from the initial slope, a change in slope is subsequently obtained for each timestep. Impacts to slope are presented for the Condamine Alluvium only as this has been identified as the primary focus area for understanding slope changes associated with CSG induced subsidence.

Two key predictive metrics are presented here, namely:

1. Predicted probability of realising a change in slope of 0.0005%, 0.001%,0.005% and 0.01%. (Figure 5-20)
2. Predicted probability of realising a maximum annual change in slope of 0.0001%/year, 0.0005%/year, 0.001%/year and 0.005%/year

Additionally, the P50 **prediction for All time maximum change in slope, Maximum Annual change in slope and year of maximum annual change in slope can be found in Appendix X.**

[4] It is acknowledged that the use of a 9 second DEM will in some situations, generalise the initial conditions. In some very local areas, baseline slope characteristics may not be represented through the use of this dataset. As such, OGIA are currently undertaking a research project to evaluate the most appropriate product and method for determining the initial conditions

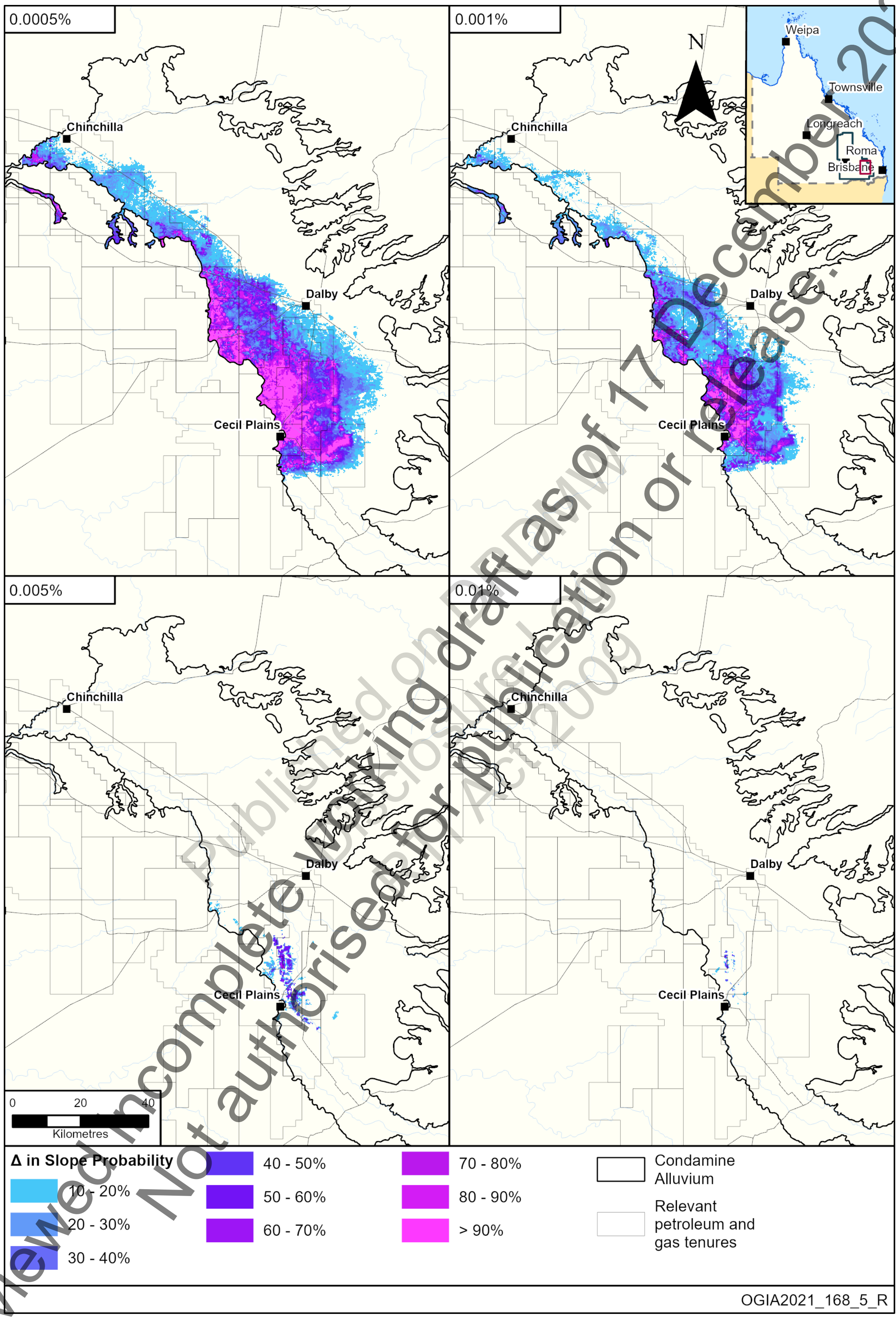

Figure 5-20 Predicted probability of realising a change in slope at any time in the future of up to a) 0.0005%, b) 001%, c)0.005% and d) 0.01%

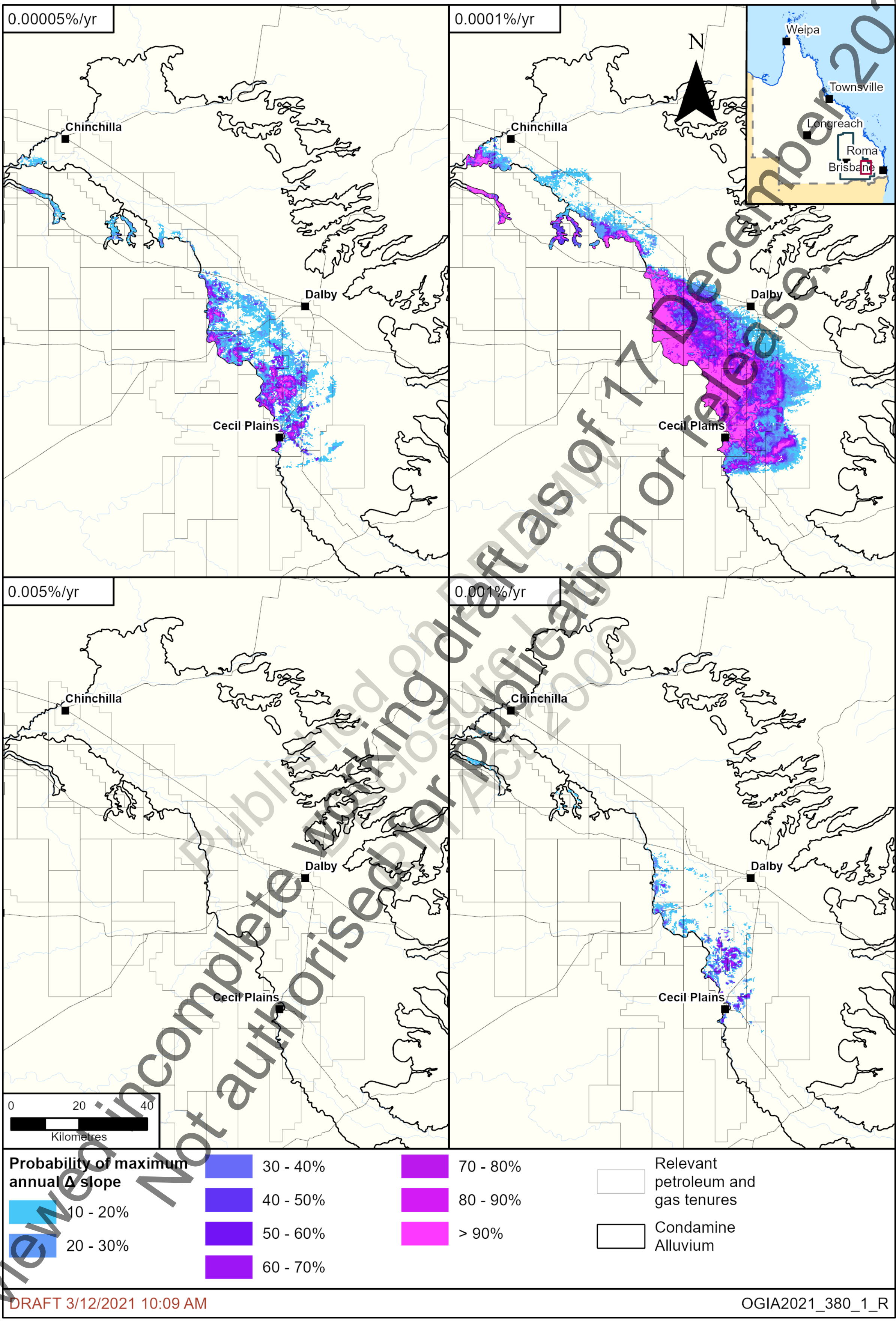

Figure 5-21 Predicted probability of realising a maximum annual change in slope at any time in the future of up to a) 0.0005%, b) 001%, c)0.005% and d) 0.01%

5 Conclusions

- CSG induced subsidence is driven by compaction processes in response to depressurisation of coal seams within CSG well fields. The degree of resulting subsidence is also controlled by the geomechanical rock properties of coal and overburden as well as the thickness and distribution of the coal.
- Monitoring techniques such as InSAR provide useful observations of change in ground elevation over time, which can be used to infer historical subsidence.
- CSG induced subsidence is observed in the Surat CMA with strong spatial correlation to existing CSG fields. Around 90 mm of downward motion is observed in active CSG areas west of Dalby.
- Background variability of +/-20 mm/y is observed in areas proximal to CSG development.
- Several additional influencing factors are identified including rainfall, soil type and land use practices.
- A subsidence model has been developed by OGIA based on available geomechanical data, calibrated to a selection of representative InSAR measurements and used for stochastic predictions of CSG induced subsidence.
- Key findings based on the 50th percentile of predictions are:
    - 90% of the affected areas are likely to experience less than 100 mm of long-term maximum subsidence; however, some areas may experience up to 200 mm.
    - 90% of the affected areas are likely to experience less than 0.001% change in slope; however, some areas may experience around 0.004% change

Reference

Commonwealth of Australia 2014, *Subsidence from coal mining activities, Background review*,.

Commonwealth of Australia 2015, *Management and monitoring of subsidence induced by longwall coal mining activity*, Prepared by Jacobs Group (Australia) for the Department of the Environment, Commonwealth of Australia, Canberra.

Department of Transport and Main Roads Queensland Government 2012, ‘Braemar Creek Bridge Foundation Investigation Report R3510’, , no. November.

Department of Transport and Main Roads Queensland Government 2014, ‘Jingi Jingi Creek Bridge Foundation Investigation Report R3543’, , no. December.

Erling Fjær, Rune Holt, Per Horsrud, AR 2008, *Petroleum Related Rock Mechanics* 2nd edn,.

Fakher, A, Cheshomi, A & Khamechiyan, M 2007, ‘The addition of geotechnical properties to a geological classification of coarse-grained alluvium in a pediment zone’, *Quarterly Journal of Engineering Geology and Hydrogeology*, vol. 40, no. 2, pp. 163–174.

GDAL/OGR 2021, ‘GDAL/OGR Geospatial Data Abstraction software Library’, *Open Source Geospatial Foundation*.

Horn, BK. 1981, ‘Hill Shading and Reflectance Map’, *IEEE*, vol. 69, pp. 14–47.

Jayeoba, A 2020, ‘Numerical simulation of ground surface subsidence due to coal-bed methane extraction’,.

Muller, S & Schuler, L ‘GeoStat-Framework/GSTools’, *Zenodo*.

OGIA 2021a, *Underground Water Impact Report 2021 for the Surat Cumulative Management Area*, Brisbane, Australia, accessed from <https://www.resources.qld.gov.au/__data/assets/pdf_file/0008/1584728/draft-uwir-2021-report.pdf>.

OGIA 2021b, *Assessment of CSG-induced subsidence in the Surat CMA (OGIA21CD19)*, Brisbane, Queensland, accessed from <https://www.business.qld.gov.au/ogia>.

Schlumberger 2021, *1D Mechanical Earth Model - Geomechanical Study to determine compaction and subsidence from Walloon Coal Measures dewatering in Condamine Alluvium area.*, Perth, Australia.

Wu, G, Jia, S & Wu, B 2019, ‘Comparison of a novel coupled hydro-mechanical model with typical analytical models in subsidence of coal seam gas extraction’,.

Wu, G, Jia, S, Wu, B & Yang, D 2018, ‘A discussion on analytical and numerical modelling of the land subsidence induced by coal seam gas extraction’, *Environmental Earth Sciences*, vol. 77, no. 9, pp. 1–13, accessed from <http://dx.doi.org/10.1007/s12665-018-7526-z>.

Appendix 1 Modelling results

Appendix 1.1 CSG and Non-CSG Subsidence

The maximum subsidence – vertical displacement (in metre), at year 2060 is predicted to range from 0.19 m to 0.23 m for the 'all combined scenario' and from 0.01 to 0.02 for the 'non-CSG' scenario, as show in Figure A3-1.

The difference between these two scenarios - equivalent to 'CSG only' scenario, display a maximum subsidence ranging from 0.19 m to 0.23 m.

Scenario at 2060	All including CSG (metre)	Non CSG (metre)
Seed 6276	0.209	0.013
Seed 2475	0.194	0.024
Seed 7377	0.224	0.016
Seed 2448	0.227	0.016

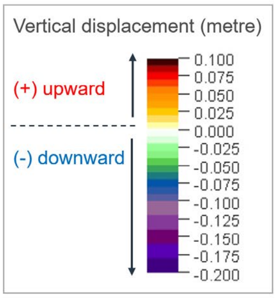

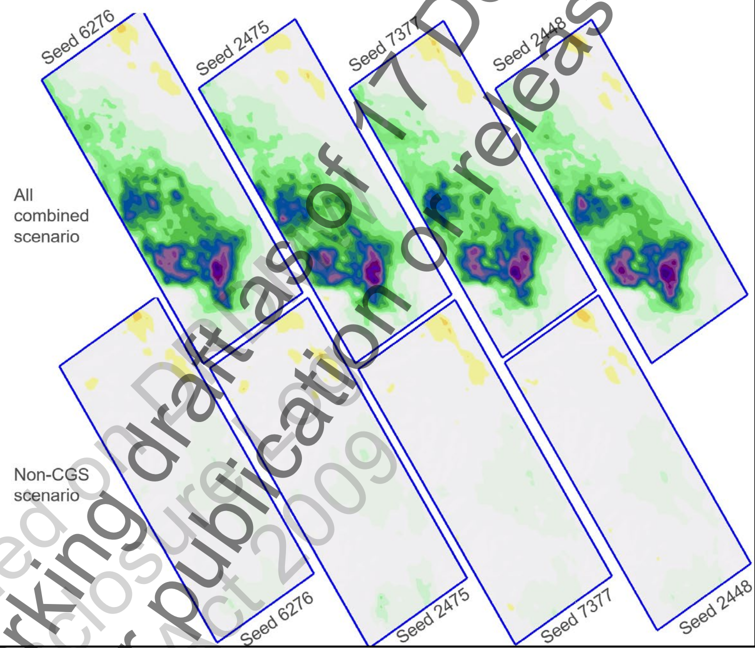

Figure A3-1: Sensitivity run results for all combined and non-CSG scenarios

Appendix 1.2 Compaction

The compaction per zone can be calculated by subtracting the vertical displacement from the top to the bottom of a formation. The majority of subsidence in the ‘CSG only’ scenario is due to compaction in the lower Juandah Coal Measures, as displayed in Figure A3-3. For the ‘non-CSG’ scenario it is related to compaction in the Cenozoic.

There is negligible overburden stress arching from the units above the Walloon Coal Measures, due to:

- very shallow overburden in comparison to the area of depletion
- the overburden zones are also depleted, although the magnitudes are smaller than that in the reservoir.

Appendix 1.3 Analytical model results

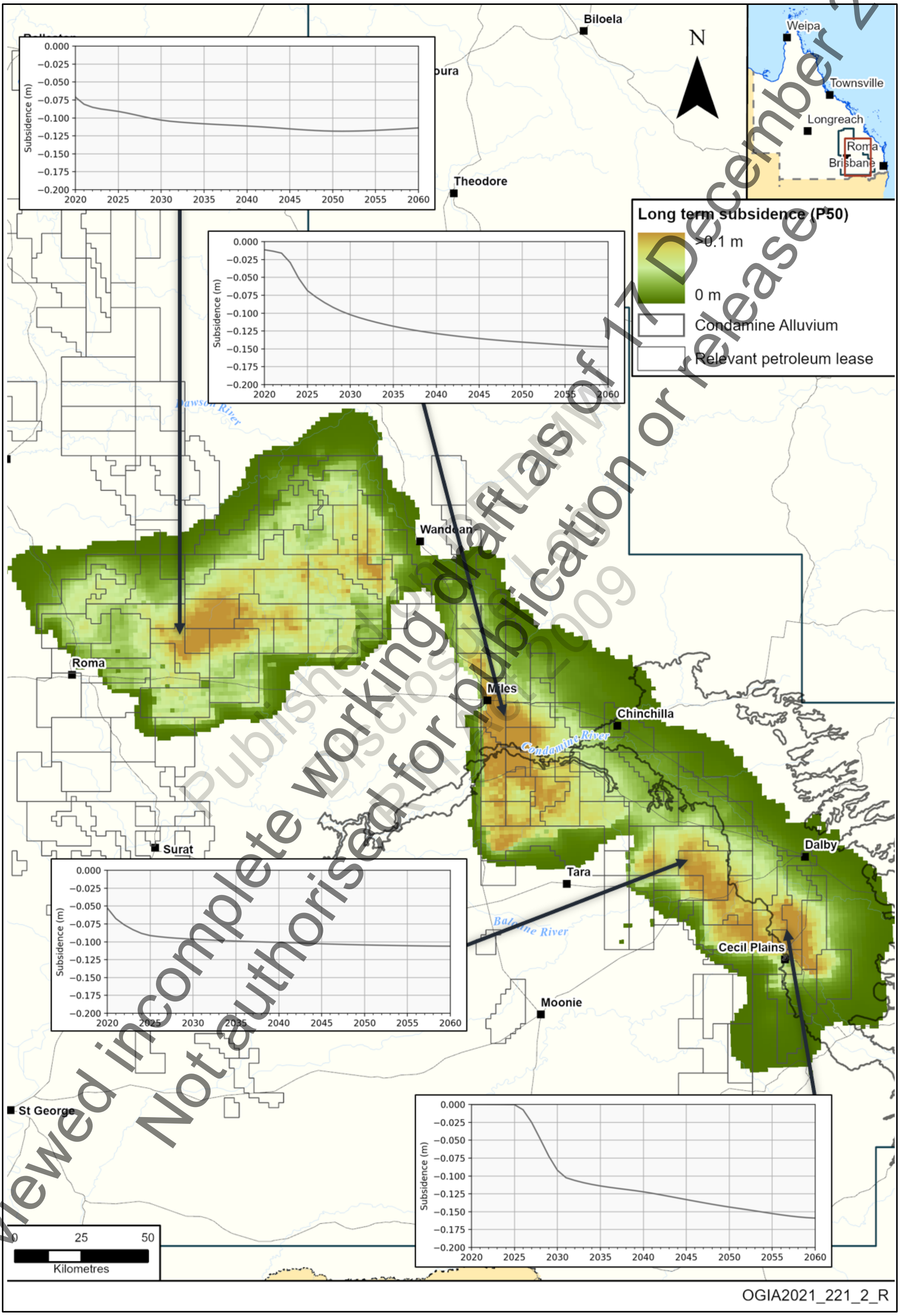

Figure 7-1 P50 prediction of CSG induced subsidence for the Surat CMA

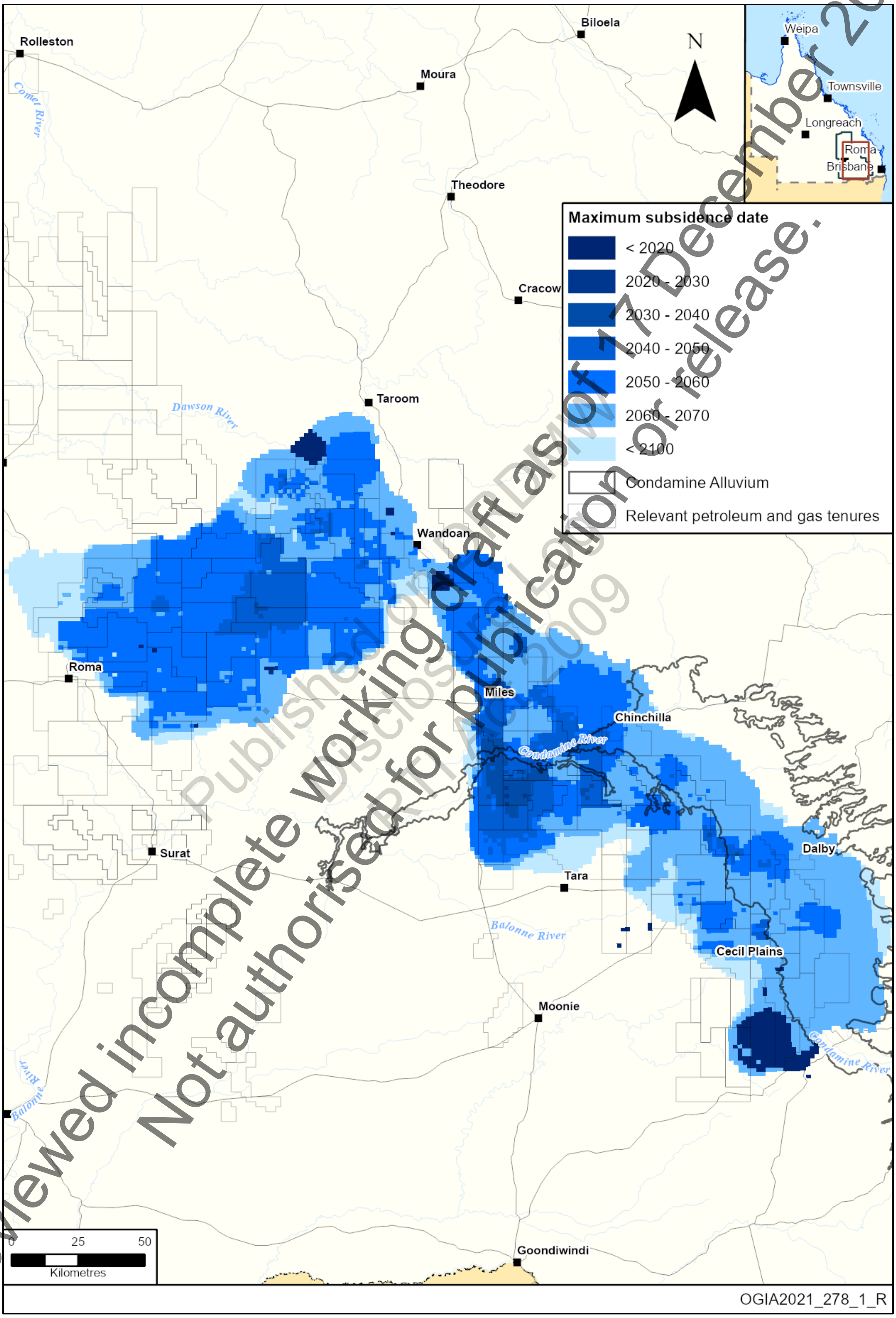

Figure 7-2 P50 Timing of Maximum Subsidence

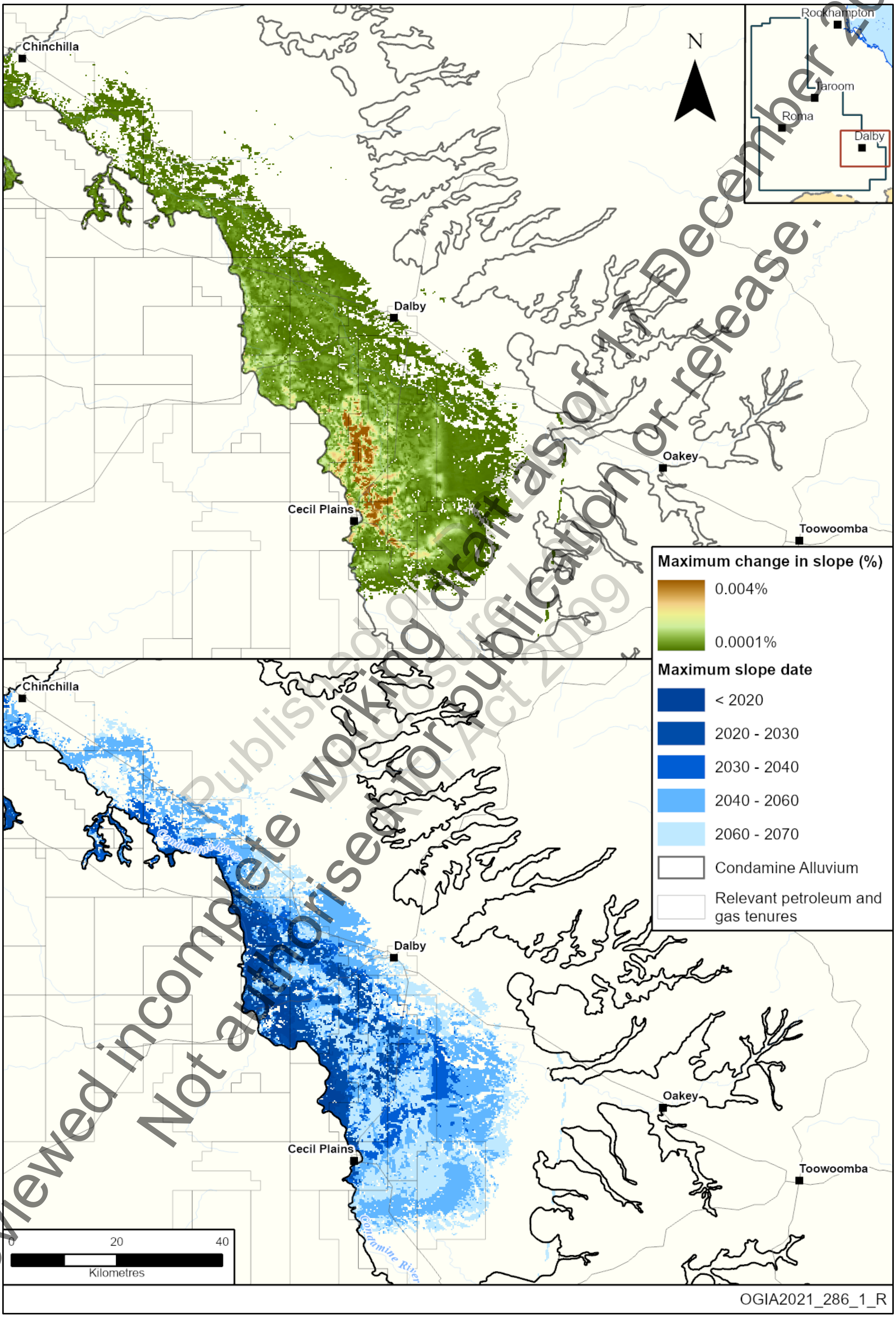

Figure 7-3 P50 Maximum change in slope and the corresponding date

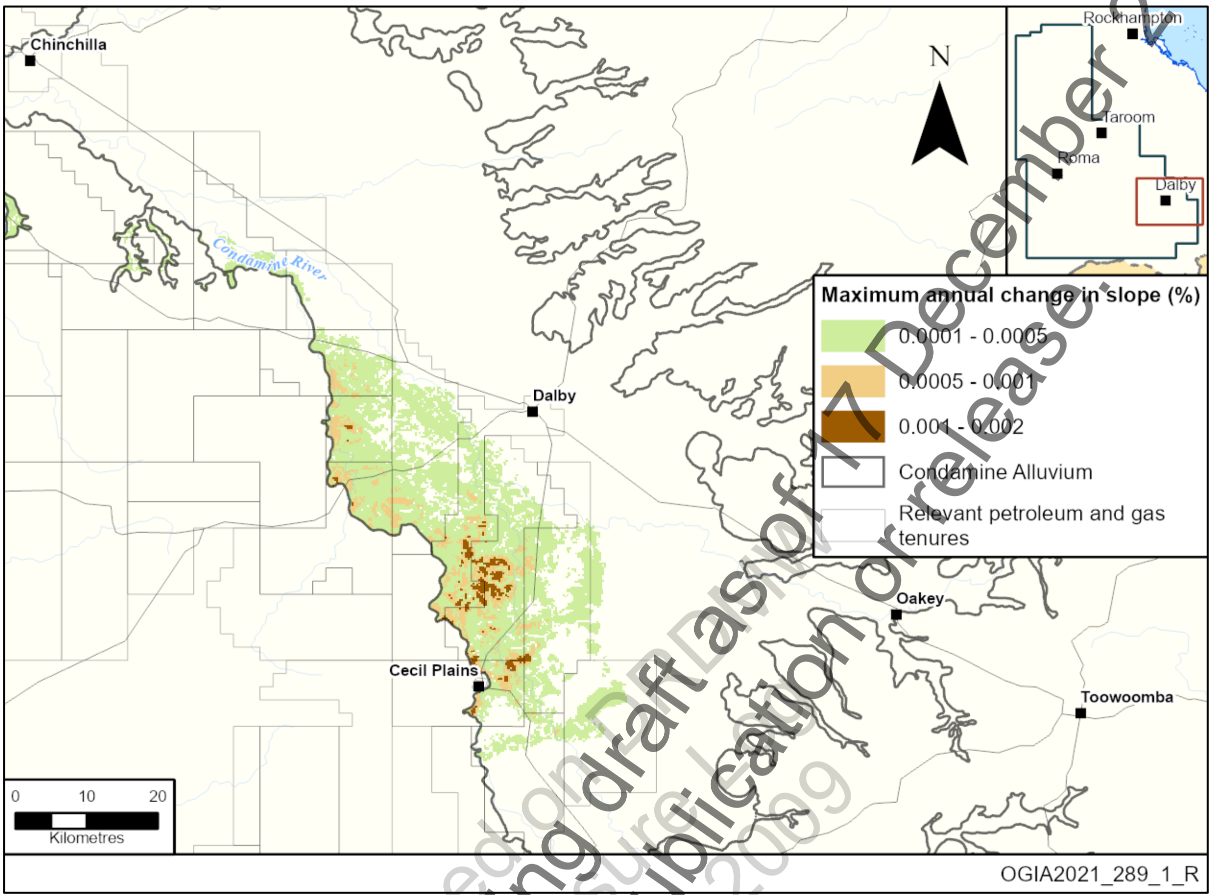

Figure 7-4 P50 Maximum annual change in slope